Misregulation of cell cycle-dependent methylation of budding yeast CENP-A contributes to chromosomal instability

Prashant K. Mishra[a], Wei-Chun Au[a], Pedro G. Castineira[a], Nazrin Ali[b], John Stanton[c], Lars Boeckmann[a,†], Yoshimitsu Takahashi[a], Michael Costanzo[d], Charles Boone[d], Kerry S. Bloom[c], Peter H. Thorpe[b], and Munira A. Basrai[a,*]

[a]Genetics Branch, National Cancer Institute, National Institutes of Health, Bethesda, MD 20892; [b]Queen Mary University of London, E1 4NS, UK; [c]University of North Carolina, Chapel Hill, NC 27599; [d]Donnelly Centre for Cellular and Biomolecular Research, University of Toronto, Toronto, ON, M5S 3E1, Canada

ABSTRACT **Centromere (*CEN*) identity is specified epigenetically by specialized nucleosomes containing evolutionarily conserved *CEN*-specific histone H3 variant CENP-A (Cse4 in *Saccharomyces cerevisiae*, CENP-A in humans), which is essential for faithful chromosome segregation. However, the epigenetic mechanisms that regulate Cse4 function have not been fully defined. In this study, we show that cell cycle-dependent methylation of Cse4-R37 regulates kinetochore function and high-fidelity chromosome segregation. We generated a custom antibody that specifically recognizes methylated Cse4-R37 and showed that methylation of Cse4 is cell cycle regulated with maximum levels of methylated Cse4-R37 and its enrichment at the *CEN* chromatin occur in the mitotic cells. Methyl-mimic *cse4-R37F* mutant exhibits synthetic lethality with kinetochore mutants, reduced levels of *CEN*-associated kinetochore proteins and chromosome instability (CIN), suggesting that mimicking the methylation of Cse4-R37 throughout the cell cycle is detrimental to faithful chromosome segregation. Our results showed that SPOUT methyltransferase Upa1 contributes to methylation of Cse4-R37 and overexpression of *UPA1* leads to CIN phenotype. In summary, our studies have defined a role for cell cycle-regulated methylation of Cse4 in high-fidelity chromosome segregation and highlight an important role of epigenetic modifications such as methylation of kinetochore proteins in preventing CIN, an important hallmark of human cancers.**

Monitoring Editor
Claire Walczak
Indiana University

Received: Mar 23, 2023
Revised: Jun 15, 2023
Accepted: Jul 06, 2023

INTRODUCTION

Accurate chromosome segregation is essential for the cell division and errors in chromosome segregation leads to chromosome instability (CIN), which is associated with several human diseases and disorders, for example cancer and developmental delays (Bakhoum and Swanton, 2014; Santaguida and Amon, 2015). Chromosome segregation in eukaryotic organisms is regulated by the kinetochore, a unique chromatin structure composed of centromeric (*CEN*) DNA, and associated protein complexes (Verdaasdonk and Bloom, 2011; Burrack and Berman, 2012; Musacchio and Desai, 2017). Despite the variations in *CEN* DNA sequences, ranging from ~125 bp of distinct DNA sequence in budding yeasts (Clarke and Carbon, 1980) to mega-base pairs of DNA representing species-specific satellite arrays, sequence repeats, or retrotransposon-derived sequences in other eukaryotic organisms (Verdaasdonk and Bloom, 2011; Musacchio and Desai, 2017), the *CEN* identity is epigenetically determined by specialized nucleosomes containing *CEN*-specific histone H3 variant, CENP-A (Cse4 in *Saccharomyces cerevisiae*, Cid in flies, and Cnp1 in fission yeast) (Sullivan *et al.*, 1994; Stoler *et al.*, 1995; Meluh *et al.*, 1998; Henikoff *et al.*, 2000; Takahashi *et al.*, 2000; Allshire and Karpen, 2008; Bui *et al.*, 2013). The epigenetic mechanisms that

This article was published online ahead of print in MBoC in Press (http://www.molbiolcell.org/cgi/doi/10.1091/mbc.E23-03-0108) on July 12, 2023.

†Present address: Clinic and Policlinic for Dermatology and Venereology, University Medical Center Rostock, 18057 Rostock, Germany

*Address correspondence to: Munira A. Basrai (basraim@nih.gov)

Abbreviations used: CEN, centromere; CIN, chromosome instability; ChIP, chromatin immunoprecipitation; END, essential N-terminus domain; FRAP, fluorescence recovery after photobleaching; GFP, green fluorescent protein; IP, immunoprecipitation; PTM, posttranslational modification; qPCR, quantitative PCR; RFP, red fluorescent protein; SL, synthetic lethality

regulate the specific localization of Cse4/CENP-A to *CEN* chromatin, and thus define *CEN*s remain to be fully characterized. One such epigenetic mechanism is the posttranslational modifications (PTMs) of Cse4 such as phosphorylation, methylation, sumoylation, and ubiquitination, which are known to regulate kinetochore function and chromosome segregation (Hewawasam *et al.*, 2010; Ranjitkar *et al.*, 2010; Samel *et al.*, 2012; Au *et al.*, 2013; Boeckmann *et al.*, 2013; Ohkuni *et al.*, 2016; Hoffmann *et al.*, 2018; Mishra *et al.*, 2019; Au *et al.*, 2020; Mishra *et al.*, 2021). For example, phosphorylation of Cse4 by protein kinases Cdc7, Cdc5, and Ipl1 modulate kinetochore integrity, chromosome biorientation, and segregation (Boeckmann *et al.*, 2013; Mishra and Basrai, 2019; Mishra *et al.*, 2019; Mishra *et al.*, 2021). Various studies have previously identified methylation of Cse4 arginine 37 (R37) in the essential N-terminus domain (END) of Cse4 (Samel *et al.*, 2012; Boeckmann *et al.*, 2013; Anedchenko *et al.*, 2019; Nguyen *et al.*, 2023). Methylation of Cse4-R37 seems to be required in the context of a defective kinetochore as *cse4-R37A* strain exhibits synthetic genetic interactions with mutants corresponding to inner kinetochore, namely COMA (Ctf19, Okp1, Mcm21, and Ame1) complex (Samel *et al.*, 2012). It has been proposed that the essential components of the COMA complex namely, Okp1 and Ame1 serve as readers for Cse4-R37 methylation, and their association with methylated Cse4-R37 acts as a signal for the loading of other kinetochore components (Anedchenko *et al.*, 2019). A recent study has shown that methylation of Cse4-lysine (K) 131 and Cse4-R143 affect the stability of *CEN* nucleosome, and their absence is detrimental when combined with the defects in the outer kinetochore proteins, such as the those of the Ndc80 complex (Nguyen *et al.*, 2023).

Previous studies have shown that dynamic reversible alterations in PTMs, such as phosphorylation-modulated kinetochore function and chromosome segregation during the cell cycle. For example, Cse4 is phosphorylated in the S-phase by Cdc7 (Mishra *et al.*, 2021), while it is phosphorylated in G2/M by Cdc5 and Ipl1 kinases (Boeckmann *et al.*, 2013; Mishra and Basrai, 2019; Mishra *et al.*, 2019). Cdc7-mediated S-phase phosphorylation of Cse4 and Cdc5-mediated mitotic phosphorylation of Cse4 contribute to kinetochore integrity and high-fidelity chromosome segregation (Mishra and Basrai, 2019; Mishra *et al.*, 2019; Mishra *et al.*, 2021), whereas Ipl1-mediated mitotic phosphorylation of Cse4 regulates kinetochore–microtubule interactions and chromosome biorientation (Boeckmann *et al.*, 2013; Mishra and Basrai, 2019). In contrast to extensive investigations for cell cycle-regulated phosphorylation of Cse4, studies to date have not examined if methylation of Cse4-R37 located within the END of Cse4 is regulated by the cell cycle and whether cell cycle-dependent methylation of Cse4-R37 affects its localization to the *CEN* chromatin and its interactions with other components of the kinetochore.

In this study, we generated a methyl-arginine 37 specific antibody (^{Me}Cse4-R37) and showed that it specifically recognizes methylated Cse4. Cell cycle stage-specific studies with the ^{Me}Cse4-R37 antibody show that methylation of Cse4-R37 is cell cycle regulated with maximum enrichment of methylated Cse4-R37 observed in mitotic cells. Chromatin immunoprecipitation (ChIP) experiments showed the association of methylated Cse4-R37 with the *CEN* chromatin. Methyl-mimic *cse4-R37F* strain exhibits defects in *CEN* localization and maintenance of kinetochore proteins, synthetic lethality (SL) with kinetochore mutants of the COMA complex, and CIN phenotype, suggesting that mimicking the methylation of Cse4-R37 throughout the cell cycle is detrimental to faithful chromosome segregation. We identified SPOUT methyltransferase Upa1 that contributes to methylation of Cse4-R37. In summary, our results provide new insights into molecular mechanisms by which misregulation of cell cycle-dependent methylation of Cse4 contributes to *CEN* dysfunction and chromosomal instability.

RESULTS

Methylation of Cse4-R37 is cell cycle regulated with maximum methylation observed in mitotic cells

Various studies have identified methylation of Cse4-R37 (Samel *et al.*, 2012; Boeckmann *et al.*, 2013), that is located within the END of Cse4 (Keith *et al.*, 1999). Mutation of Cse4-R37 to cse4-R37A does not affect chromosome segregation, however, methylation of Cse4-R37 is important in the context of a defective kinetochore. For example, the *cse4-R37A* strain exhibits genetic interactions with mutants of kinetochore genes, such as those encoding for the components of the COMA complex (Samel *et al.*, 2012). Notably, Cse4 is one of the key factors that regulates kinetochore architecture and its structural changes during mitosis, which are important for faithful chromosome segregation (Yeh *et al.*, 2000; Wisniewski *et al.*, 2014; Hara and Fukagawa, 2020). Hence, we sought to define the dynamics and physiological significance of Cse4-R37 methylation through the cell cycle. To facilitate the detection of Cse4-R37 methylation, we generated a methyl-arginine 37 specific antibody (^{Me}Cse4-R37) and tested its specificity using endogenously expressed HA-Cse4 or HA-cse4-R37A expressed from their native promoters at the endogenous locus. The ^{Me}Cse4-R37 antibody detected methylated Cse4 in wild-type *HA-CSE4* strain, but reactivity was not observed in *HA-cse4-R37A* strain (Figure 1A; Supplemental Figure S1, A and B). These results show that the ^{Me}Cse4-R37 antibody preferentially recognizes methylated Cse4-R37 thereby providing an ideal tool for further studies. To determine whether methylation of Cse4-R37 is cell cycle regulated, we assayed methylation of endogenously expressed HA-Cse4 in wild-type cells that were synchronized in G1 (α-factor treatment), S (hydroxyurea treatment) or G2/M (nocodazole treatment) stages of the cell cycle. The cell cycle stage was confirmed by flow cytometry, nuclear position and cell morphology analyses (Figure 1B; Supplemental Figure S1C). Maximum enrichment of methylated Cse4-R37 was observed in G2/M cells compared with that observed in the S-phase cells, whereas it was barely detectable in G1 cells (Figure 1C). We quantified the fraction of methylated Cse4-R37 (^{Me}HA-Cse4) and normalized this to total Cse4 levels (HA-Cse4) in each stage of the cell cycle using the procedure described previously (Mishra *et al.*, 2015). The enrichment of methylated Cse4-R37 was significantly higher (three to fivefold) in mitotic (G2/M) cells than the G1 or S-phase cells (Figure 1D). Based on these observations, we conclude that methylation of Cse4-R37 is cell cycle regulated, which is primarily observed in mitotic cells and to some extent, in S-phase cells.

We next performed cell cycle arrest-release experiment to confirm the methylation pattern of Cse4-R37. Cells were synchronized in G1 (α-factor treatment) and released into pheromone-free media (Figure 2, A, B, and C). Based on the flow cytometry profiles (Supplemental Figure S2A), nuclear position, and cell morphology (Figure 2C), cells were categorized as G1, S, metaphase, anaphase, and telophase as described previously (Calvert and Lannigan, 2010; Mishra *et al.*, 2011; Mishra *et al.*, 2021). Consistent with results from Figure 1,C and D, methylation of Cse4-R37 was barely detectable in G1 cells (20 min post release from α-factor arrest), observed in S-phase cells (40 min post release from α-factor arrest), and was highly enriched in mitotic cells (60–100 min post release from α-factor arrest) (Figure 2, A and B). The highest enrichment of methylated Cse4-R37 was observed in metaphase cells (Figure 2, B and C).

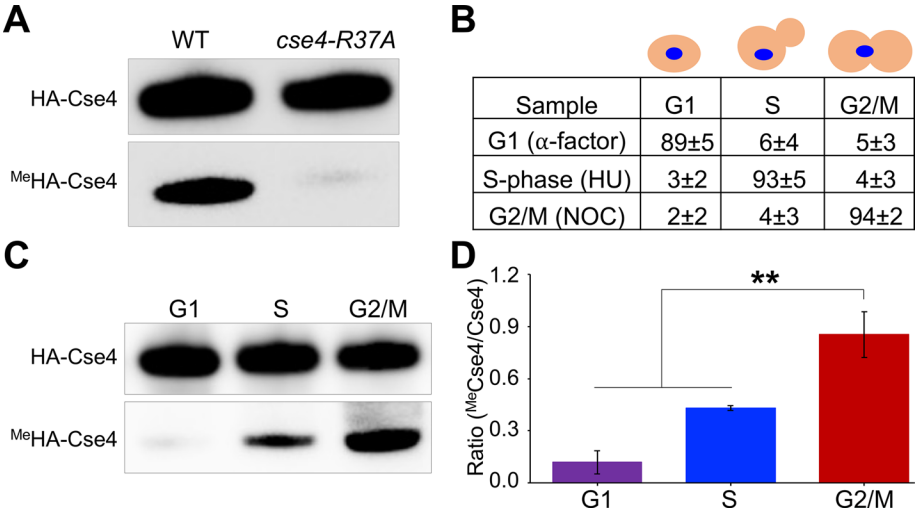

FIGURE 1: Methylation of Cse4-R37 is cell cycle regulated. (A) Specificity of ^{Me}Cse4-R37 antibodies to methylated Cse4. Western blots showing specific reactivity of the ^{Me}Cse4-R37 antibodies. Cse4 was enriched with Ni-NTA agarose from whole cell extracts of logarithmically growing wild-type (YMB7289) and *cse4-R37A* (YMB7287) strains and analysed by Western blotting using α-HA and α-^{Me}Cse4-R37 antibodies. (B) Cell morphology analysis show synchronization in G1, S-phase and G2/M. Wild-type strain (YMB7289) was grown to early logarithmic phase at 25°C and synchronized in G1 (3-μM α-factor treatment), S-phase (0.2-M HU treatment), and G2/M (20-μg/mL NOC treatment). Cell cycle stages were determined based on nuclear position and cell morphology by microscopic examination of at least 100 cells for each sample. Different stages of the cell cycle: G1, S-phase (S), and G2/M. Average ± standard error (SE) derived from three biological replicates is shown. (C) The levels of methylated Cse4-R37 are higher in G2/M (mitotic) cells. Cse4 was enriched with Ni-NTA agarose using whole cell extracts from wild-type strain (YMB7289) synchronized in G1, S-phase, and G2/M and analysed by Western blotting using α-HA and α-^{Me}Cse4 antibodies. (D) Enrichment of relative methylation of Cse4 in G1, S-phase, and G2/M. Ratio of methylated Cse4-R37 (^{Me}HA-Cse4) to the total Cse4 (HA-Cse4) was calculated using Image J (Schneider *et al.*, 2012). Three biological replicates were done. Average ± SE is shown. ***p* value < 0.01, Student's *t* test.

Based on these results, we conclude that methylation of Cse4-R37 is cell cycle regulated.

Methylated Cse4 associates with the *CEN* chromatin

The increased methylation of Cse4-R37 in mitotic cells led us to examine if methylated Cse4 associates with the *CEN* chromatin. This was done by ChIP experiments using chromatin from wild-type *HA-CSE4* and *HA-cse4-R37A* strains synchronized with nocodazole in the G2/M phase of the cell cycle (Supplemental Figure S2B) and antibodies to HA-Cse4 and ^{Me}Cse4-R37. Western blotting showed that expression of HA-Cse4 and HA-cse4-R37A is similar in these two strains (Figure 2D; Supplemental Figure S2C). ChIP-quantitative PCR (qPCR) showed that the levels of *CEN*-associated HA-Cse4 were similar between wild-type (3.5% at *CEN1*, and 3.2% at *CEN3*) and *HA-cse4-R37A* (3.8% at *CEN1*, and 3.24% at *CEN3*) strains (Figure 2E). However, ^{Me}Cse4-R37 levels at *CEN* were significantly lower in *HA-cse4-R37A* (0.07% at *CEN1*, and 0.08% at *CEN3*) than in wild-type (0.37% at *CEN1*, and 0.38% at *CEN3*) strain (Figure 2F). No significant enrichment of Cse4 or ^{Me}Cse4-R37 was observed at non-*CEN ACT1* locus used as a negative control. These results show that methylated Cse4 associates with *CEN* chromatin in mitotic cells.

Reduced association of methyl mimic Cse4-R37F with *CEN* chromatin and kinetochores

We constructed a *cse4-R37F* strain in which Cse4-R37 was replaced with phenylalanine (F) because F mimics methylarginine and contains similar size of hydrocarbon chains and bulky hydrophobic moieties observed for methylarginine (Mostaqul Huq *et al.*, 2006; Paik *et al.*, 2007; Dillon *et al.*, 2013). Several studies have used substitution with F for mimicking the constitutive methylation of arginine residue in a range of organisms (Mostaqul Huq *et al.*, 2006; Bikkavilli and Malbon, 2011; Dillon *et al.*, 2013; Yan *et al.*, 2018; Zhong *et al.*, 2018; Angrand *et al.*, 2022; Wang *et al.*, 2023). ChIP experiments were done to examine the association of HA-tagged protein in G2/M cells of wild-type *HA-CSE4* and mutant *HA-cse4-R37A* and *HA-cse4-R37F* strains. Cell cycle synchronization in G2/M was confirmed by flow cytometry profiles and examination of nuclear position and cell morphology (Supplemental Figure S3, A and B). ChIP-qPCR showed that the enrichment of HA-Cse4 and HA-cse4-R37A at *CEN* chromatin (*CEN1* and *CEN3*) is not significantly different (*p* value = > 0.05; Figure 3A). However, enrichment of HA-cse4-R37F at *CEN* chromatin was significantly reduced (~1.5% of input) when compared with the levels observed for HA-Cse4 (~2.7% of input; Figure 3A). No significant enrichment of HA-Cse4, HA-cse4-R37A, or HA-cse4-R37F was detected at the non-*CEN ACT1* locus used as a negative control (Figure 3A). Western blotting showed that the protein levels of HA-Cse4, HA-cse4-R37A, or HA-cse4-R37F were similar (Figure 3B; Supplemental Figure S3C).

We next used a cell-biology approach to quantify the intensity of green fluorescent protein (GFP)-Cse4 at the kinetochore using fluorescence imaging in wild-type strain and in mutants expressing GFP-cse4-R37A or GFP-cse4-R37F. Discrete GFP-Cse4 foci consistent with kinetochore localization were observed for wild-type and mutants. However, the intensity of GFP-cse4-R37F foci was reduced when compared with that observed for GFP-Cse4 or GFP-cse4-R37A foci (Figure 3C). We quantified the fluorescence intensity of the GFP-foci using the Foci Quant script in the Image J (Schneider *et al.*, 2012). This analysis revealed significantly reduced levels (*p* value = 2.8×10^{-23}) of GFP-cse4-R37F fluorescence intensity (1289.8 ± 687.7, mean ± SD) when compared with that observed for GFP-Cse4 (1876.6 ± 954.3) or GFP-cse4-R37A (2408.9 ± 776.4; Figure 3D).

The reduced association of cse4-R37F at *CEN* chromatin and kinetochores prompted us to examine whether the turnover and exchange of cse4-R37F were also affected at the *CEN* chromatin using a Fluorescence Recovery After Photobleaching (FRAP) assay (Pearson *et al.*, 2004). Consistent with cell biology results (Figure 3D), the GFP fluorescence intensities at the metaphase kinetochore of wild-type GFP-Cse4 were higher than that for GFP-cse4-R37F (wild-type = 123.5, cse4-R37F = 102.2). The metaphase kinetochores decorated with GFP-foci representing GFP-Cse4 or GFP-cse4-R37F were photobleached and FRAP (pre and post) was measured. The average GFP fluorescence recovery at 10 min post photobleaching in the *cse4-R37F* strain was 9.8%, which is markedly higher than that observed for the wild-type strain (~5.4%). Moreover, a pairwise *t* test

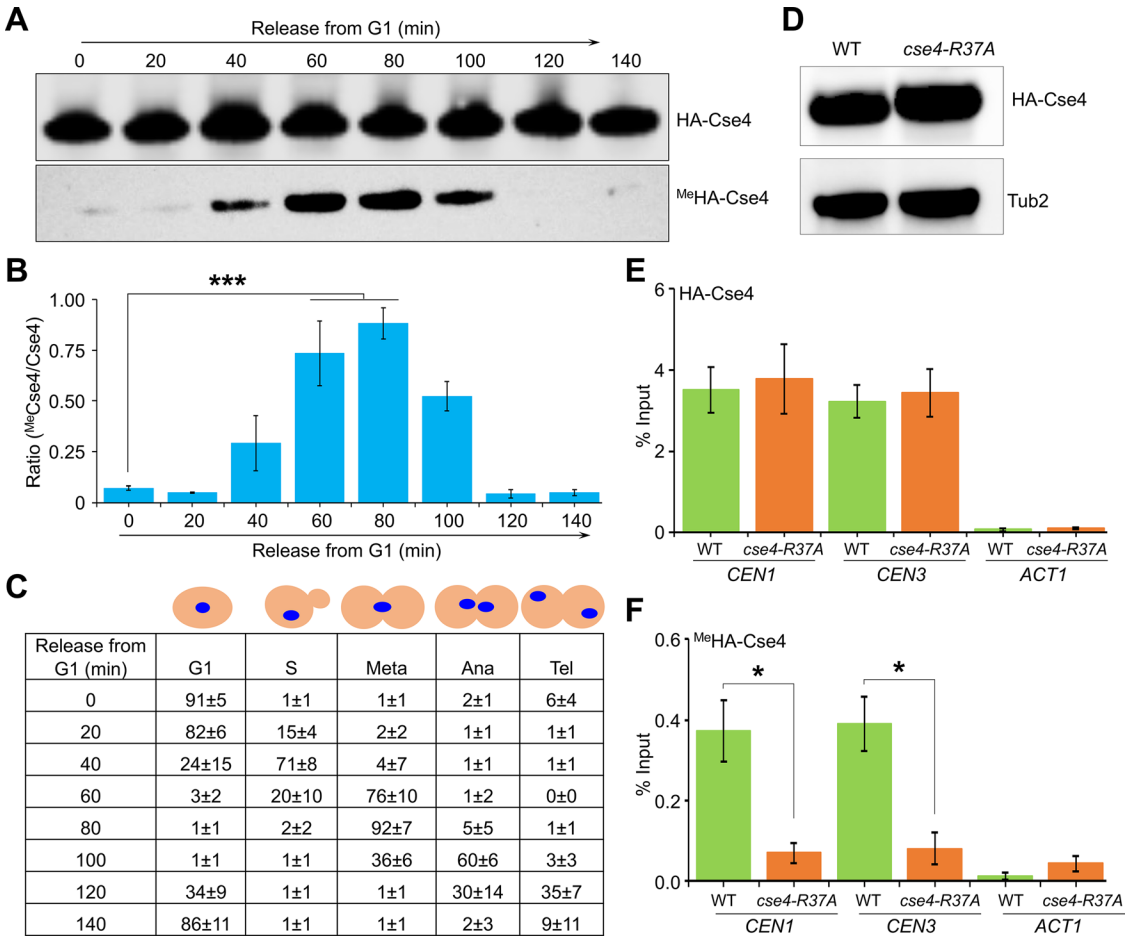

Release from G1 (min)	G1	S	Meta	Ana	Tel
0	91±5	1±1	1±1	2±1	6±4
20	82±6	15±4	2±2	1±1	1±1
40	24±15	71±8	4±7	1±1	1±1
60	3±2	20±10	76±10	1±2	0±0
80	1±1	2±2	92±7	5±5	1±1
100	1±1	1±1	36±6	60±6	3±3
120	34±9	1±1	1±1	30±14	35±7
140	86±11	1±1	1±1	2±3	9±11

FIGURE 2: Methylated Cse4-R37 is highly enriched and associates with *CEN* chromatin in mitotic cells. (A) Enrichment of methylated Cse4-R37 increases during the mitosis. Wild-type strain (YMB10574) grown in YPD at 25°C to early logarithmic phase and synchronized in G1 with α-factor, released into pheromone-free medium, and sampled at 20 min time intervals. α-factor was readded at 80 min to block cells in next G1. Cse4 was enriched with Ni-NTA agarose from whole cell extracts and analysed by Western blotting using α-HA and α-^{Me}Cse4-R37 antibodies. Western blots show the levels of Cse4 (HA-Cse4) and methylated Cse4-R37 (^{Me}HA-Cse4) during the cell cycle. (B) Enrichment of relative methylation of Cse4-R37 during the cell cycle. Ratio of methylated Cse4-R37 (^{Me}HA-Cse4) to the total Cse4 (HA-Cse4) was determined with Image J (Schneider *et al.*, 2012). Average from three biological replicates ± SE. ***p value < 0.001, Student's t test. (C) Cell cycle stages were determined based on nuclear position and cell morphology by microscopic examination of at least 100 cells for each sample. Different stages of the cell cycle: G1, S-phase (S), metaphase (Meta), anaphase (Ana) and Telophase (Tel). Average ± SE derived from three biological replicates is shown. (D) Protein levels of Cse4 and cse4-R37A are largely similar in G2/M cells. Wild-type (WT; YMB10574) and *cse4-R37A* (YMB11651) strains were grown to early logarithmic phase at 25°C and synchronized with nocodazole in G2/M. Western blotting of protein extracts using α-HA and α-Tub2 (loading control) antibodies. (E and F) Methylated Cse4-R37 associates with *CEN* chromatin in G2/M. ChIP was performed in WT (YMB10574) and *cse4-R37A* (YMB11651) strains from (D) using α-HA agarose and α-^{Me}Cse4-R37 antibodies. Enrichment of Cse4 and ^{Me}Cse4-R37 at *CENs* (*CEN1* and *CEN3*) and a negative control (*ACT1*) was determined by qPCR and is shown as % input. Average from three biological replicates ± SE. *p value < 0.05, Student's t test.

comparison of GFP-fluorescence intensities post photobleaching revealed a significant difference between wild-type and *cse4-R37F* strains (p value = 0.015, Supplemental Table S1). Taken together, these observations suggest that methyl mimic cse4-R37F affects its stable maintenance at the kinetochores with reduced levels at the *CEN* chromatin.

Methyl mimic *cse4-R37F* strain exhibits defects in kinetochore and CIN phenotype

Previous studies have shown that Mif2 (CENP-C in humans), a part of the inner kinetochore associates with Cse4 and is present at *CEN* chromatin (Brown *et al.*, 1993; Meluh and Koshland, 1995; Cohen *et al.*, 2008; Ho *et al.*, 2014). The reduced *CEN* association of cse4-R37F led us to examine whether *CEN* localization of Mif2 is also reduced in *cse4-R37F* strain. ChIP experiments were done to assay the *CEN* levels of Mif2 in wild-type, *cse4-R37A*, and *cse4-R37F* strains synchronized in G2/M (Supplemental Figure S3, A and B). ChIP-qPCR showed that the enrichment of Mif2 at *CEN* chromatin (*CEN1* and *CEN3*) is largely similar and not significantly different between wild-type and *cse4-R37A* strains (p value = > 0.05; Figure 4A). However, enrichment of Mif2 at *CEN* was significantly reduced in *cse4-R37F* (~1.7–1.9% of input) when compared with the wild-type (~3.2% of

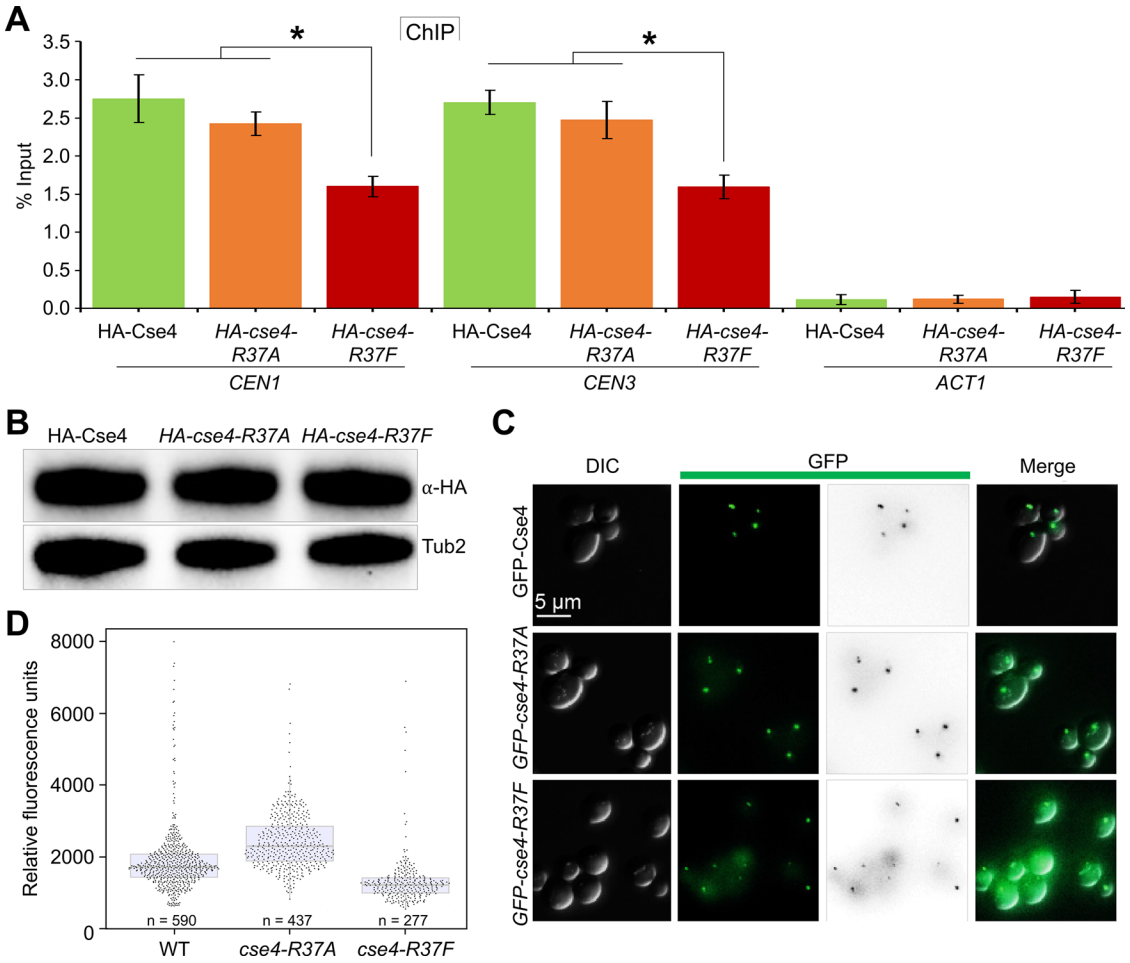

FIGURE 3: Reduced association of methyl mimic cse4-R37F with *CEN* chromatin and kinetochores. (A) Levels of cse4-R37F are reduced at *CEN* chromatin. Wild-type (WT, YMB10574), *cse4-R37A* (YMB11651) and *cse4-R37F* (YMB11652) strains were grown to early logarithmic phase at 25°C and synchronized with nocodazole in G2/M and ChIP was performed using α-HA agarose antibodies. Enrichment of Cse4 and its mutants at *CENs* (*CEN1* and *CEN3*) and a negative control (*ACT1*) was determined by qPCR and is presented as % input. Average from three biological replicates ± SE. **p* value < 0.05, Student's *t* test. (B) Expression of Cse4, cse4-R37A and cse4-R37F. Western blotting of protein extracts from strains in (A) using α-HA and α-Tub2 (loading control) antibodies. (C) Reduced association of GFP-cse4-R37F at the kinetochore. Representative images showing GFP-Cse4 fluorescence at the kinetochores in wild-type (T785), *cse4-R37A* (T786) and *cse4-R37F* (T796) strains. (D) Quantitation of GFP fluorescence intensity from strain imaged in panel (C). GFP-signals were quantified using Image J and analysed in R-Studio. *n* = the number of cells examined.

input; *p* value = < 0.05; Figure 4A) strain. No significant enrichment of Mif2 was detected at the non-*CEN ACT1* locus used as a negative control (Figure 4A). Western blotting showed that the protein levels of Mif2 were similar in wild-type, *cse4-R37A*, and *cse4-R37F* strains (Figure 4B; Supplemental Figure S3D).

Based on the results for defects in kinetochore integrity in *cse4-R37F* strains (Figures 3 and 4), we hypothesized that mimicking the continuous methylation of Cse4-R37 throughout the cell cycle will contribute to defective chromosome segregation. We constructed *cse4-R37A* and *cse4-R37F* strains carrying a reporter chromosome fragment (CF) and determined the frequency of CF loss which results in red sectors in an otherwise white colony (Spencer *et al.*, 1990) The frequency of CF loss in the first division (half red-half white colonies) was not significantly different between wild-type and *cse4-R37A* strains (*p* value = 0.52; Figure 4C). Notably, the frequency of CF loss was significantly higher (about 15-fold; *p* value = 0.0083; Figure 4C) in *cse4-R37F* strain than in the wild-type strain and the increased CF loss of *cse4-R37F* strain is similar to that described for other kinetochore mutants(Kastenmayer *et al.*, 2005; Ma *et al.*, 2012). We noted that Cse4-R37 is substituted by a K residue in some fungal species carrying point *CEN* (Supplemental Figure S4A). Given that K can also be a substrate residue for methylation, we hypothesized that the *cse4-R37K* strain may not exhibit defects in chromosome segregation. Consistent with this hypothesis, CF loss was not observed in the *cse4-R37K* strain (Supplemental Figure S4B). Taken together, we conclude that methyl mimic cse4-R37F contributes to defects in kinetochore integrity and CIN.

cse4-R37F strain exhibits synthetic growth defects with kinetochore mutants

We performed a genome-wide genetic screen using a synthetic genetic array (SGA) to identify gene deletions or mutants that display SL with *cse4-R37F* strain. A query strain with *cse4-R37F* integrated at the endogenous *CSE4* locus was mated to an array of nonessential (~4293 gene deletions) and essential (~786 conditional TS alleles) genes, and the growth of the haploid meiotic progeny of each mutant

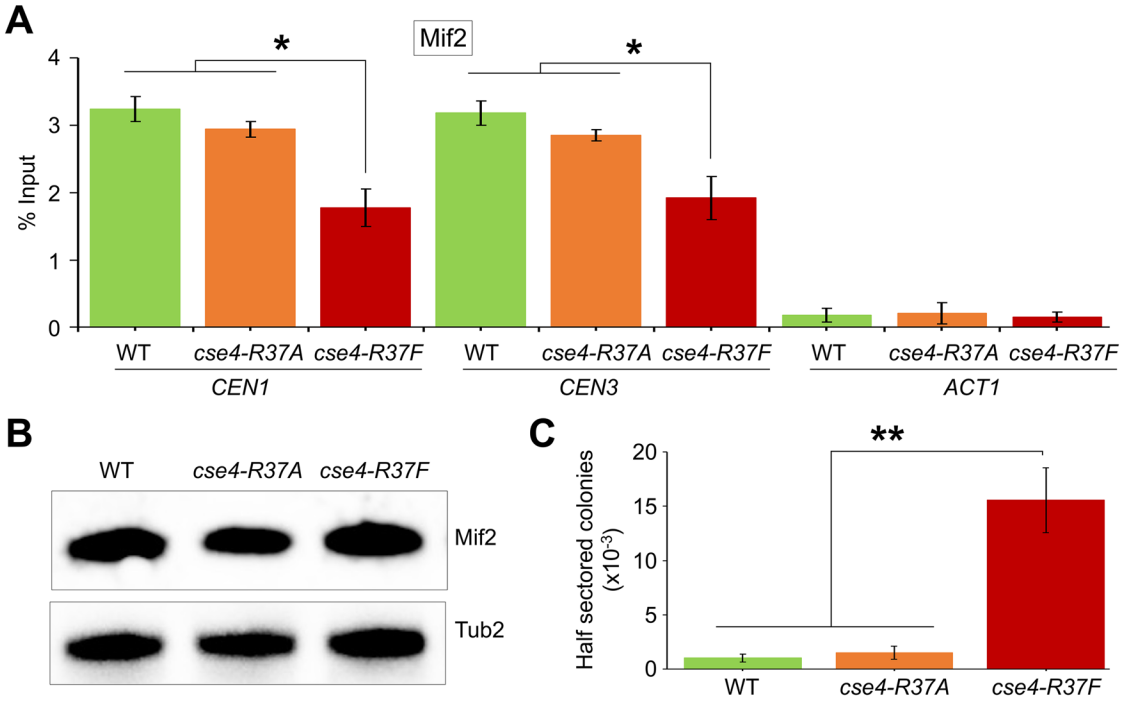

FIGURE 4: Methyl mimic *cse4-R37F* strain exhibits defects in kinetochore integrity and CIN phenotype. (A) Levels of Mif2 are reduced at *CEN* chromatin in *cse4-R37F* strains. ChIP was performed with α-Mif2 antibodies using chromatin from strains in Figure 3A. Enrichment of Mif2 at *CENs* (*CEN1* and *CEN3*) and a negative control (*ACT1*) was determined by qPCR and is presented as percent input. Average from three biological replicates ± SE. **p* value < 0.05, Student's *t* test. (B) Expression of Mif2 in wild-type, *cse4-R37A*, and *cse4-R37F* strains. Western blotting of protein extracts from strains in Figure 3A using α-Mif2 and α-Tub2 (loading control) antibodies. (C) Methyl mimic *cse4-R37F* strain exhibits CIN. Frequency of CF loss in wild-type (WT; YPH1015), *cse4-R37A* (YMB11649), and *cse4-R37F* (YMB11650) was determined as described in *Materials and Methods*. At least 1000 colonies each from three independent transformants were counted. Values are average ± SE. ***p* value < 0.01, Student's *t* test.

carrying *cse4-R*37F was measured at the permissive temperature of 26°C. The SGA score for growth was calculated as defined previously (Baryshnikova *et al.*, 2010; Wagih *et al.*, 2013) and filtered based on the intermediate confidence threshold values (*p* value < 0.05 and

[Score] >0.08; Costanzo *et al.*, 2010; Costanzo *et al.*, 2016). The SGA showed that mutants corresponding to 188 essential and 368 nonessential genes exhibited significant negative genetic interaction with *cse4-R37F* strain (Supplemental Table S2). Gene Ontology (GO) analysis of the negative genetic interactors for biological processes and cellular components was performed using FunSpec software with a cutoff value of ≤0.05 (http://funspec.med.utoronto.ca/). GO identified categories related to kinetochore, chromosome segregation, cell division, mitosis, and chromosomes (Figure 5A). A majority of the negative interactor genes are related to kinetochore function and chromosome segregation representing the components of COMA (Ctf19, Okp1, Mcm21, Ame1), DAM1 (e.g., Dam1, Dad1), MIND (e.g., Dsn1), and Ndc80 (e.g., Spc24) complexes (Supplemental Table S2). We validated the results of SGA by genetic analysis and tetrad dissection of a subset of kinetochore mutants (KAN^{+R}) with *cse4-R37F* (NAT^{+R}). We observed SL of cse4-R37F with mutants of the COMA complex as both the *cse4-R37F ame1-4* and *cse4-R37F ctf19*Δ double mutants were inviable as KAN^{+} NAT^{+} progeny was not observed and the two *cse4-37F mcm21*Δ mutants that we recovered showed very slow growth (Figure 5, B and C). We also validated genetic interaction of *cse4-R37F* with mutant that corresponds to microtubule-associated protein Irc15 where only two of 10 expected *cse4-R37F irc15*Δ mutants and five of 10 expected *cse4-R37F mad1*Δ mutants were viable (Figure 5B). The viable spores in these strains largely exhibit synthetic sick (slow growth) phenotype. In contrast to *cse4-R37F*, SL was not observed in *cse4-R37K* when combined with the deletion of a component of the COMA complex, Ctf19 (Supplemental Figure S4C). Overall, SGA screen for SL with *cse4-R37F* and nonessential and essential gene mutants revealed an enrichment of genes that regulate kinetochore function and faithful chromosome segregation.

cse4-R37F strain exhibits reduced levels of kinetochore proteins Ctf19 and Ame1 at *CEN* chromatin

The results of SGA and validation by analysis of meiotic progeny confirmed SL of *cse4-R37F* with mutants corresponding to components of the COMA complex namely, Ctf19 and Ame1 (Figure 5). We posit that *cse4-R37F* strains may exhibit reduced association of Ctf19 and Ame1 at *CEN* chromatin. Hence, we examined the *CEN* levels of Ctf19 and Ame1 in G2/M cells of wild-type and mutant strains (Supplemental Figure S3). In agreement with our hypothesis, ChIP-qPCR showed that the enrichment of Ctf19 at *CEN* was reduced significantly in *cse4-R37F* strain (~0.12–0.17% of input) when compared with the wild-type (~0.39% of input; Figure 6A). Similarly, *CEN* levels of Ame1 were also reduced significantly in *cse4-R37F* strain (~1.0% of input) than the levels observed for the wild-type strain (~2.4% of input; Figure 6B). The enrichment of Ctf19 or Ame1 at *CEN* chromatin (*CEN1* and *CEN3*) was not significantly different between wild-type and *cse4-R37A* strains (*p* value = > 0.05; Figure 6, A and B). No significant enrichment of Ctf19 or Ame1 was detected at the non-*CEN ACT1* locus used as a negative control (Figure 6, A and B).

A

GO Term	Non-essential Genes			Essential Genes		
	Gene Name	Fraction	*p* value	Gene Name	Fraction	*p* value
Cellular Component:						
Kinetochore	*IML3 CHL4 MCM21 NKP1 CNN1 MAD1 MCM22 NKP2 CTF3 CTF19 MCM16*	11/48	$4.84e^{-05}$	*STU1 AME1 DAD1 SPC19 SPC105 DAM1 OKP1 CRM1 TID3 DSN1 NNF1 STU2 SPC24 NUF2 IPL1 NSL1*	16/48	$9.34e^{-14}$
Chromosome	*IML3 CHL4 MCM21 NKP1 CNN1 SKI8 ZIP2 EST3 MCM22 NKP2 CTF3 YKU70 CTF19 MCM16*	14/130	0.0130	*STU1 AME1 DAD1 STN1 SPC19 SPC105 DAM1 CBF2 OKP1 TID3 DSN1 SMC3 NNF1 SMC4 CTF13 SPC24 CEP3 NUF2 IPL1 NSL1*	20/130	$4.88e^{-10}$
Biological process:						
Chromosome segregation	*IML3 PAT1 CHL4 MCM21 CNN1 ZIP2 MCM22 CTF3 CTF19 MCM16*	10/69	0.0045	*DAD1 DBF4 SPC19 GLC7 SCC4 ESP1 DAM1 CBF2 OKP1 TID3 DSN1 NNF1 SDS22 SPC24 NUF2 IPL1 NSL1*	17/69	$4.21e^{-12}$
Cell division	*IML3 PAT1 CHL4 MCM21 NKP1 CNN1 MAD1 MAD2 BFA1 MCM22 NDL1 NKP2 CTF3 DNL4 CTF19 CLN2 MCM16*	17/190	0.0354	*STU1 CDC27 AME1 CDC7 KIN28 DAD1 DBF4 CDC37 SPC19 GLC7 SCC4 CDC26 SRM1 CDC20 DAM1 OKP1 TID3 DSN1 SMC3 CDC11 NNF1 SDS22 SMC4 CDC3 TEM1 SPC24 NUF2 APC5 NSL1*	29/190	$1.00e^{-14}$
Mitosis	*IML3 CHL4 MCM21 NKP1 CNN1 MAD1 MAD2 BFA1 MCM22 NDL1 NKP2 CTF3 CTF19 MCM16*	14/132	0.0148	*STU1 CDC27 AME1 CDC7 DAD1 DBF4 SPC19 GLC7 SCC4 CDC26 SRM1 CDC20 DAM1 OKP1 TID3 DSN1 SMC3 NNF1 SDS22 SMC4 TEM1 SPC24 NUF2 APC5 NSL1*	25/132	$1.88e^{-14}$

B

cse4-R37F x	Tetrads dissected	Double mutants	Kinetochore complex/ component
ame1-4	10	0	COMA complex
ctf19Δ	9	0	COMA complex
mcm21Δ	9	2	COMA complex
irc15Δ	10	2	Spindle
chl4Δ	10	4	Outer kinetochore
mad1Δ	10	5	Checkpoint

C

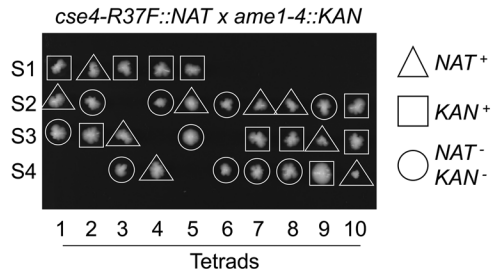

FIGURE 5: Methyl mimic *cse4-R37F* strains exhibits negative genetic interactions with chromosome segregation mutants. (A) GO analysis of the negative genetic interactors for biological process and cellular component based on SGA of *cse4-R37F* with nonessential and essential gene mutations. (B) Methyl mimic *cse4-R37F* strains exhibits negative genetic interactions with *ame1-4*, *ctf19*Δ, *mcm21*Δ, *irc15*Δ, *chl4*Δ, and *mad1*Δ. Analysis of meiotic progeny of tetrad analysis from mating of *cse4-R37F* with isogenic BY4741 strains carrying mutations in kinetochore components as indicated. The number of expected and observed double mutants observed are shown. (C) Representative image from tetrad dissection showing SL when *cse4-R37F* was combined with kinetochore mutant *ame1-4*. The four spores (S1–S4) from individual asci and their genotypes are marked.

Western blot analysis showed similar levels of protein expression of Ctf19 and Ame1 in wild-type and mutant strains (Figure 6, C and D; Supplemental Figure S3, E and H). These results show that *cse4-R37F* strain has reduced *CEN* association of kinetochore proteins Ctf19 and Ame1 and this may contribute to the CIN phenotype of *cse4-R37F* strain (Figure 4C) and SL phenotype when *cse4 R37-F* is combined with kinetochore mutants (Figure 5).

Evolutionarily conserved SPOUT methyltransferase Upa1 contributes to Cse4 methylation

A previous study showed that strains deleted for genes encoding arginine methyltransferases (Hmt1, Rmt2, and Hsl7) do not show reduced methylation of Cse4-R37 or exhibit the synthetic growth defects when combined with *cbf1*Δ or *ctf19*Δ strains (Samel *et al.*, 2012) suggesting that methylation of Cse4-R37 is likely catalyzed by an uncharacterized methyltransferase(s). Notably, previous studies have identified a novel role for SPOUT (SpoU-TrmD) methyltransferases in protein arginine methylation in budding yeast (Wlodarski *et al.*, 2011; Young *et al.*, 2012). Moreover, human SPOUT methyltransferase protein 1 (also known as CENP32) associates with the kinetochore (Ohta *et al.*, 2015) and its depletion exhibits negative genetic interaction with a deletion of *CEN* protein (CENP-P; Horlbeck *et al.*, 2018), a phenotype that is analogous to SL observed in *cse4-R37A* strains when combined with the deletion of CENP-P homologue in budding yeast, Ctf19 (Samel *et al.*, 2012). Remarkably, deletion of Upa1 (yeast homologue of CENP32) also exhibits negative genetic interactions and growth defects with the kinetochore mutants (Costanzo *et al.*, 2010; Costanzo *et al.*, 2016). Moreover, Upa1 interacts in vivo and in vitro with kinetochore protein Cbf5 (Jiang *et al.*, 1993; Krogan *et al.*, 2004; Schwer *et al.*, 2011; Snider *et al.*, 2014; Ismail *et al.*, 2022) and is an active component of preprimordial 60S pre-ribosome (Ismail *et al.*, 2022). Based on these observations, we hypothesized that Upa1 may have a role in Cse4-R37 methylation. Hence, we examined the levels of Cse4-R37 methylation in wild-type and *upa1*Δ strains synchronized in G2/M (Supplemental Figure S5). Western blot analysis showed that ^{Me}Cse4-R37 was significantly reduced in *upa1*Δ (~40% reduction) when compared with the wild-type strain (Figure 7, A and B). The reduction in ^{Me}Cse4-R37 is linked to *upa1*Δ strain as the defect in methylation is complemented by a plasmid expressing *UPA1* from its native promoter (Figure 7, A and B). Consistent with a role for *UPA1* in Cse4-R37 methylation, overexpression of *UPA1* resulted in significant increase in the levels of ^{Me}Cse4-R37 in G2/M but not in G1 cells (Figure 7, C and D; Figure S6). Moreover, strains overexpressing

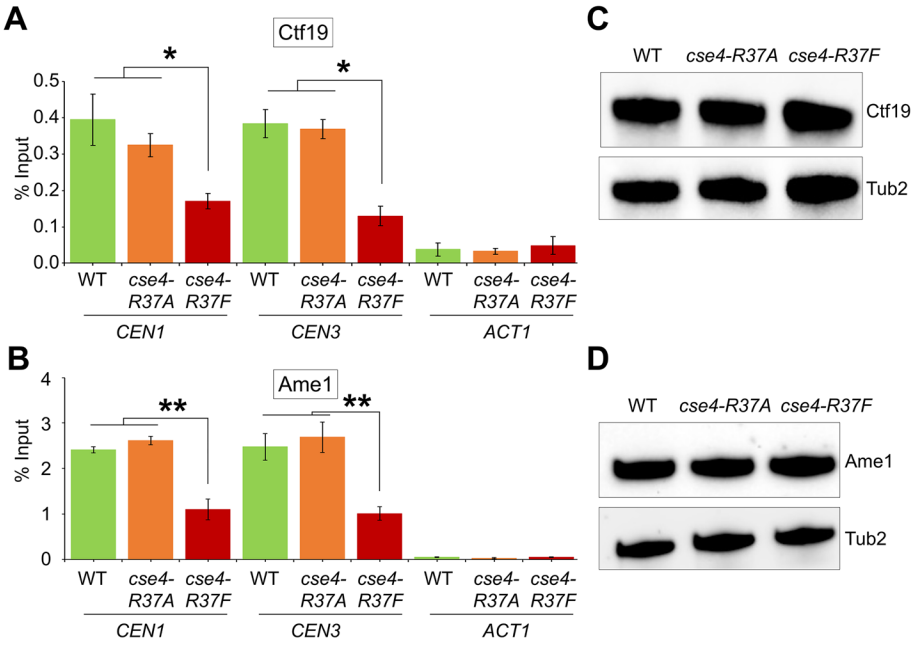

FIGURE 6: Reduced *CEN* association of kinetochore proteins Ctf19 and Ame1 in methyl mimic *cse4-R37F* strain. (A) Levels of Ctf19 are reduced at *CEN* chromatin in *cse4-R37F* strains. ChIP was performed with α-Ctf19 antibodies using chromatin from same strains as used in Figure 3A. Enrichment of Ctf19 at *CENs* (*CEN1* and *CEN3*) and a negative control (*ACT1*) was determined by qPCR and is presented as % input. Average from three biological replicates ± SE. **p* value < 0.05, Student's *t* test. (B) Levels of Ame1 are reduced at *CEN* chromatin in *cse4-R37F* strains. ChIP was performed with α-Myc agarose antibodies using chromatin from wild-type (WT, YMB11828), *cse4-R37A* (YMB11829), and *cse4-R37F* (YMB11830) strains grown to early logarithmic phase at 25°C and synchronized with nocodazole in G2/M. Enrichment of Ame1 at *CENs* (*CEN1* and *CEN3*) and a negative control (*ACT1*) was determined by qPCR and is presented as % input. Average from three biological replicates ± SE. ***p* value < 0.01, Student's *t* test. (C) Expression of Ctf19 in wild-type, *cse4-R37A*, and *cse4-R37F* strains are similar. Western blotting of protein extracts was done using α-Ctf19 and α-Tub2 (loading control) antibodies. (D) Expression of Ame1 in wild-type, *cse4-R37A*, and *cse4-R37F* strains are similar. Western blotting of protein extracts was done using α-Myc (Ame1) and α-Tub2 (loading control) antibodies.

UPA1 exhibit increased CF loss in a wild-type strain (Figure 7E). To determine whether the CF loss phenotype is due to increased methylation of Cse4-R37, we compared CF of *GALUPA1* in wild-type and *cse4-R37A* strains. Our results showed that CF loss was significantly reduced in a *cse4-R37A* strain upon *UPA1* overexpression (Figure 7E). Taken together, these results suggest that SPOUT methyltransferase Upa1 contributes to Cse4-R37 methylation.

DISCUSSION

Evolutionarily conserved *CEN*-specific histone H3 variant, Cse4 and its homologues are considered as an epigenetic mark for kinetochore identity and are essential for faithful segregation of chromosomes during the cell-division cycle (Sullivan *et al.*, 1994; Stoler *et al.*, 1995; Meluh *et al.*, 1998; Henikoff *et al.*, 2000; Takahashi *et al.*, 2000; Allshire and Karpen, 2008). Recent studies have highlighted the role of Cse4 PTMs in its regulation, kinetochore function and chromosome segregation (Hewawasam *et al.*, 2010; Ranjitkar *et al.*, 2010; Samel *et al.*, 2012; Au *et al.*, 2013; Boeckmann *et al.*, 2013; Ohkuni *et al.*, 2016; Hoffmann *et al.*, 2018; Mishra *et al.*, 2019; Au *et al.*, 2020; Mishra *et al.*, 2021). Methylation of Cse4 arginine residue at position 37 has been identified and proposed to have a role in kinetochore assembly (Samel *et al.*, 2012; Boeckmann *et al.*, 2013; Anedchenko *et al.*, 2019). However, the dynamics of Cse4-R37 methylation through the cell cycle and its impact on kinetochore structure and function have not been characterized. Here, we report that Cse4-R37 methylation is cell cycle regulated with maximum enrichment observed in mitotic cells and methylated Cse4-R37 associates with the *CEN* chromatin. The studies with methyl mimic *cse4-R37F* strain revealed: a) synthetic growth defects when combined with kinetochore mutants such as those corresponding to COMA complex, b) reduction and faster exchange of cse4-R37F at the kinetochore, c) reduction in the levels of *CEN*-associated kinetochore proteins Mif2, Ctf19, and Ame1, and d) increased frequency of chromosome loss. In addition, we have identified a novel role for SPOUT methyltransferase Upa1 in methylation of Cse4-R37. Based on these results, we propose a model in which cell cycle-dependent methylation of Cse4-R37 regulates faithful chromosome segregation and its misregulation contributes to defects in kinetochore structure and function leading to CIN (Figure 8).

We provide the first evidence for cell cycle regulation for methylation of Cse4-R37. The abundance of methylated Cse4-R37 increases from S-phase to G2/M cells and decreases rapidly in cells arrested in G1, implying a high degree of coordination between the cell cycle and Cse4-R37 methylation. Previous studies have shown that Cse4 recruitment to the kinetochore is regulated by the cell cycle and its exchange at the kinetochore occurs during the early S-phase when old Cse4 molecules are replaced by the new Cse4 molecules (Pearson *et al.*, 2004; Wisniewski *et al.*, 2014). The seeding of new Cse4 molecules at the kinetochore in the S-phase is essential for subsequent assembly of other components of the kinetochore, spindle, microtubules, and other factors associated with the process of chromosome segregation (Yeh *et al.*, 2000; Yeh *et al.*, 2008; Wisniewski *et al.*, 2014; Bloom and Costanzo, 2017; Lawrimore *et al.*, 2018). Methylation of Cse4-R37 has been proposed to be recognized by kinetochore proteins Okp1 and Ame1, which in turn serves as a signaling mechanism for subsequent assembly of other kinetochore components (Anedchenko *et al.*, 2019). Our observation showing enrichment of methylated Cse4-R37 in S-phase cells is consistent with the proposed role of Cse4-R37 methylation in kinetochore assembly. However, the maximum enrichment of methylated Cse4-R37 was detected in mitotic cells, suggesting that Cse4-R37 methylation may have additional mitotic roles at the budding yeast kinetochore. Precedence for this is based on studies with human cells in which arginine methylation of regulator of chromatin condensation 1 (RCC1) protein modulates spindle formation and chromosome segregation (Clarke, 2021; Huang *et al.*, 2021). Similarly, arginine methylation of ubiquitin-associated protein 2-like (UBAP2L) is necessary for proper alignment of chromosomes in metaphase and is required for correct kinetochore–microtubule attachment for the error-free progression of the mitosis (Maeda *et al.*, 2016). Moreover, arginine methylation of Rad9 plays an important role in S and

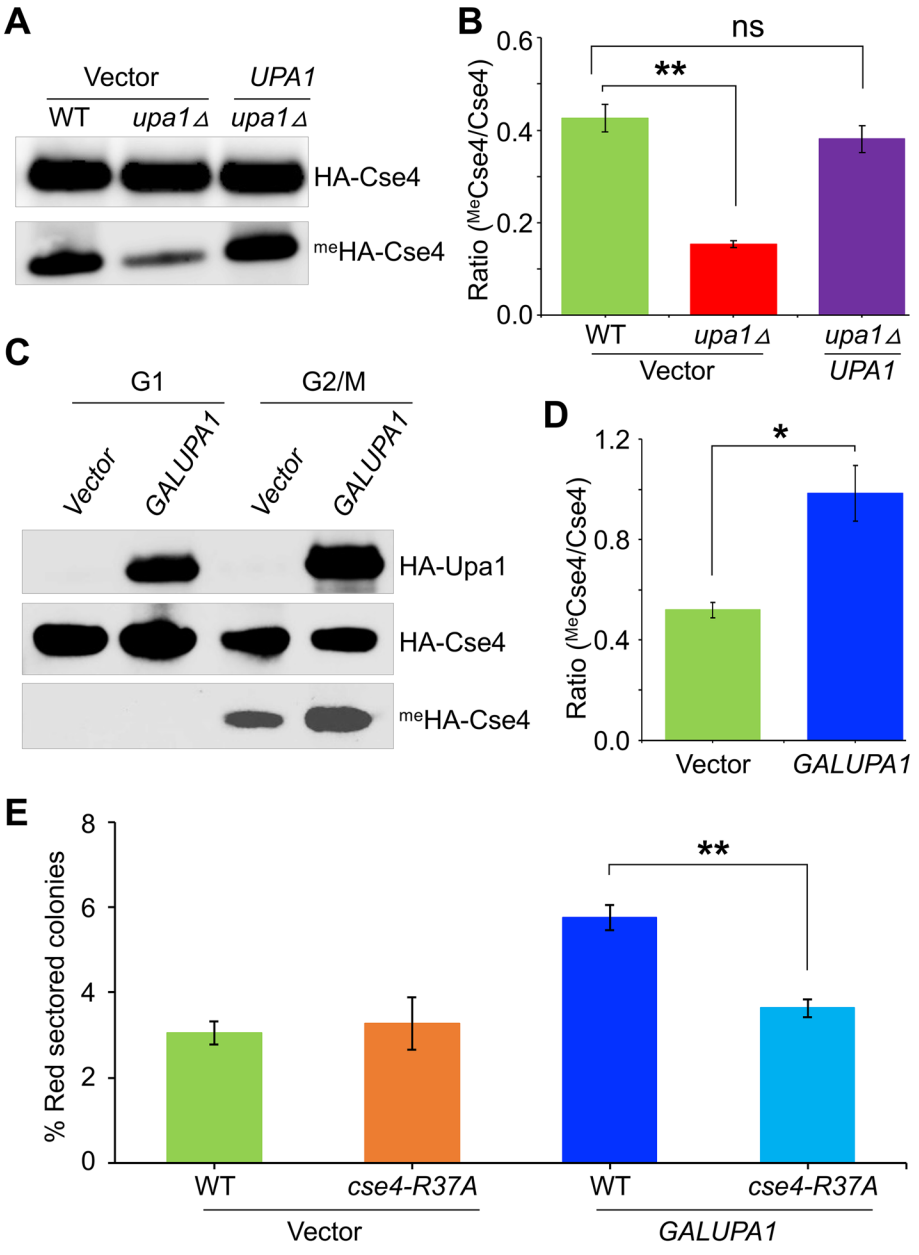

FIGURE 7: SPOUT methyltransferase Upa1 contributes to methylation of Cse4-R37. (A) Reduced levels of methylated Cse4-R37 in *upa1*Δ strain. Western blot analysis of extracts prepared from logarithmically grown wild-type (WT) strain with vector (YMB11880) and *upa1*Δ strain with vector (YMB11881) or *2μ UPA1* (YMB11882) were analysed by α-HA (HA-Cse4) and α-^{Me}Cse4-R37 (^{Me}HA-Cse4) antibodies. (B) Reduced methylation of Cse4-R37 in *upa1*Δ strain is complemented by plasmid based *UPA1*. Quantification of relative methylation of Cse4 of strains from (A). Ratio of methylated Cse4 (^{Me}HA-Cse4) to the total Cse4 (HA-Cse4) was calculated using Image J. Three biological replicates were done. Average ± SE is shown. **p value < 0.01, ns = statistically not significant, Student's t test. (C) Increased methylation of Cse4-R37 in mitotic cells of *UPA1* overexpressing strain. Western blot analysis of Ni-NTA agarose immunoprecipitated extracts from wild-type (WT) strain with vector (YMB11878) or *GAL1-6HIS-HA-UPA1* (YMB11879) strain grown in SC-Ura with galactose + raffinose (2% each) at 25°C for 6 h, synchronized in G2/M with nocodazole and analysed using α-HA (HA-Cse4 or HA-Upa1) and α-^{Me}Cse4-R37 (^{Me}HA-Cse4) antibodies. (D) Quantification of relative methylation of Cse4 of strains from (C). Ratio of methylated Cse4-R37 (^{Me}HA-Cse4) to the total Cse4 (HA-Cse4) was calculated using Image J. Three biological replicates were done. Average ± SE is shown. *p value < 0.05, Student's t test. (E) Overexpression of *UPA1* causes errors in chromosome segregation. Frequency of CF loss in wild-type with vector (YMB12214) or *GAL1-6HIS-HA-UPA1* (YMB12215) and *cse4-R37A* strain with vector (YMB12217) or *GAL1-6HIS-HA-UPA1* (YMB12218) was determined as described in *Materials and Methods*. At least 1000 colonies each from three independent transformants were counted. Average ± SE is shown. **p value < 0.01, Student's t test.

G2/M cell cycle progression and checkpoint activation (He *et al.*, 2011). Future studies will allow us to define the physiological significance of methylated Cse4-R37 in mitosis.

A recent study has identified methylation within the C-terminus of Cse4 (K131 and R143), which affects the stability of *CEN* nucleosomes in the context of defects in outer kinetochore proteins, such as those of the Ndc80 complex (Nguyen *et al.*, 2023). Although both C- and N-terminus methylation of Cse4 exhibit negative genetic interactions with kinetochore mutants and defects in *CEN* integrity, there is a distinction in which they affect the kinetochore structure and function. The phenotypes for the C-terminus methylation were observed when combined with mutations in the outer kinetochore component (Nguyen *et al.*, 2023), whereas the phenotypes for N-terminus methylation were detected when combined with mutations in the inner kinetochore components, such as COMA complex (Samel *et al.*, 2012; Anedchenko *et al.*, 2019). It is possible that the C- and the N-terminus methylation of Cse4 could be controlled differentially by the cell cycle in a manner that coordinates the assembly of kinetochore components and faithful chromosome segregation. Moreover, various studies have shown that Cse4 is modified by both phosphorylation and methylation (Samel *et al.*, 2012; Boeckmann *et al.*, 2013; Anedchenko *et al.*, 2019; Mishra and Basrai, 2019; Mishra *et al.*, 2019; Mishra *et al.*, 2021). Notably, methylated Cse4-R37 is flanked by two of the phosphorylated residues, S33 and S40 (Boeckmann *et al.*, 2013; Mishra and Basrai, 2019), however relationships between these two PTMs of Cse4 and their physiological significance for chromosome segregation remain to be investigated. Studies from budding yeast and other systems have highlighted the importance of the crosstalk between PTMs in determining their activity and function (Zhang *et al.*, 2005; Fang *et al.*, 2014; Liu *et al.*, 2020; Smith *et al.*, 2020). For example, methylation of kinetochore protein Dam1 by Set1 methyltransferase inhibits its phosphorylation by Ipl1 kinase, which is critical for faithful chromosome segregation and cell viability (Zhang *et al.*, 2005). It is of great interest to examine for possible crosstalk between phosphorylation and methylation of Cse4.

The *cse4-R37A* mutant exhibits no observable phenotype unless it is combined with the kinetochore mutants (Samel *et al.*, 2012; Anedchenko *et al.*, 2019). The lack of any detectable phenotype in *cse4-R37A*

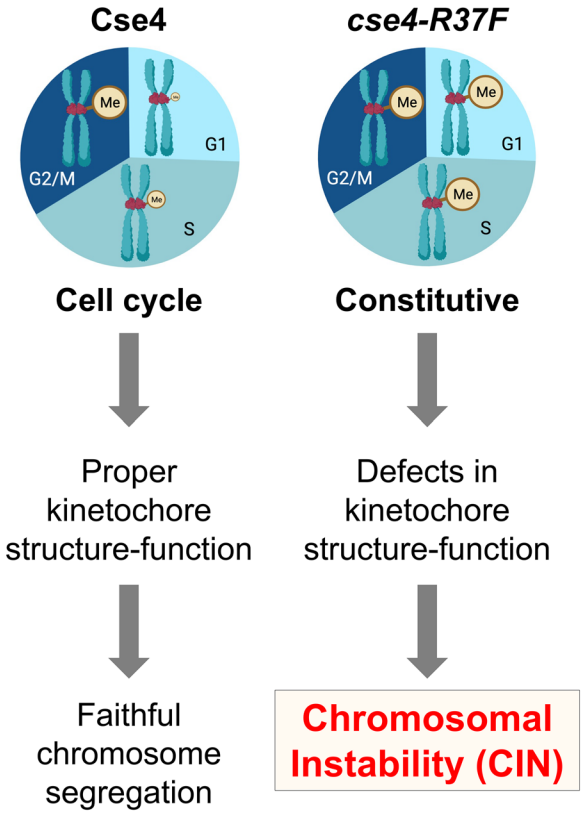

FIGURE 8: Cell cycle-regulated methylation of Cse4-R37 prevents CIN. In wild-type (Cse4) strains, cell cycle-regulated Cse4 methylation modulates proper kinetochore structure and function leading to faithful chromosome segregation, whereas in methyl mimic *cse4-R37F* strains exhibit defects in kinetochore structure and function leading to CIN. The model was created with BioRender.com.

could be due to compensatory effect produced by the methylation of R143 in the C-terminus of Cse4 (Nguyen *et al.*, 2023) or other methylated arginine residues in Cse4 that are yet to be identified. In this study we show that the *cse4-R37F* mutant, which mimics methylation of Cse4-R37 throughout the cell cycle shows SL with kinetochore mutants, such as COMA complex. The assembly of COMA complex at the kinetochore occurs via its interaction with the N-terminus of Cse4, which subsequently facilitates the recruitment of Sli15/Ipl1 to the kinetochore for the fidelity of spindle assembly checkpoint and chromosome biorientation (Hornung *et al.*, 2014; Anedchenko *et al.*, 2019; Fischbock-Halwachs *et al.*, 2019). When combined with the kinetochore mutants, the absence (*cse4-R37A*) or mimic of methylation (*cse4-R37F*) may interfere with the integrity of the mitotic spindle, which likely contributes to growth defects and SL phenotypes.

Although both *cse4-R37F* and *cse4-R37A* mutants exhibit growth defects and SL with kinetochore mutants, several phenotypes were uniquely observed in the *cse4-R37F* mutant, for example, reduction in *CEN* levels of kinetochore proteins such as, Ame1, Ctf19, Mif2, including cse4-R37F, a faster exchange of cse4-R37F at the metaphase kinetochore, and increased frequency of CIN. Apparently, mimicking the methylation of Cse4-R37 throughout the cell cycle (*cse4-R37F*) shows much stronger phenotypic defects than the absence of Cse4-R37 methylation (*cse4-R37A*). One of the contributing mechanisms for this observation could be disruption of the dynamic cell cycle-dependent regulation of Cse4-R37 methylation. Mimicking the presence of methylation in G1 or the lack of demethylation in late mitosis (late anaphase and telophase) possibly creates an epigenetic chromatin environment at the kinetochore that is not ideal for faithful chromosome segregation. The presence of methylation in G1 could interfere with the assembly of kinetochore proteins in the S-phase, whereas the lack of demethylation in late mitosis may affect the processes of error corrections caused by faulty kinetochore–microtubule attachments. Moreover, depletion of *CEN* levels of cse4-R37F and its faster exchange at the kinetochore indicate that cse4-R37F is a less stable protein and cannot remain stably associated with the kinetochore. The depletion of Cse4 from *CEN* has previously been shown to increase the accumulation of negative DNA supercoils at the *CEN* DNA (Henikoff and Furuyama, 2010; Huang *et al.*, 2011; Henikoff and Furuyama, 2012; Mishra *et al.*, 2013; Vlijm *et al.*, 2017) leading to topological defects that interfere with the downstream assembly of kinetochore components, cell cycle progression, and checkpoint function, and these observations were associated with kinetochore dysfunction and CIN (Haase *et al.*, 2013; Mishra *et al.*, 2013). It is intriguing to speculate that reduction in *CEN* associated cse4-R37F could potentially contribute to accumulation of negative DNA supercoils at the *CEN* leading to increased frequency of CIN as observed in *cse4-R37F* mutant. We surmise that these events either individually or collectively contribute to defects in the kinetochore in *cse4-R37F* strains. Taken together, we propose that the mimicking methylation of Cse4-R37 throughout the cell cycle may interfere with the ordered assembly of kinetochore components and trigger incorrect geometric positioning and defective kinetochore orientation during mitosis, all of which are essential for faithful chromosome segregation (Yeh *et al.*, 2000; Sprague *et al.*, 2003; Watanabe, 2012; Bloom and Costanzo, 2017; Lawrimore *et al.*, 2018; Lawrimore and Bloom, 2019).

A previous study did not reveal a role for arginine methyltransferases Hmt1, Rmt2, and Hsl7 in methylation of Cse4-R37 (Samel *et al.*, 2012). We have now identified SPOUT methyltransferase Upa1 that contributes to the methylation of Cse4-R37. The level of Cse4-R37 methylation was reduced upon deletion of *UPA1*, while it was increased upon *UPA1* overexpression. Although SPOUT methyltransferases are largely known to modify RNAs, recent studies have defined their role in protein arginine methylation (Wlodarski *et al.*, 2011; Krishnamohan and Jackman, 2019). Notably, Spout Family Methyltransferase 1 (Sfm1) methylates arginine 146 of Rps3 protein in budding yeast, which is required for the import of Rps3 protein to the nucleolus for assembly of the ribosomal small subunit (Young *et al.*, 2012). The methylation of Rps3-R146 is physiologically important as its absence (*rps3-R146A*) affects cellular growth and fitness (Young *et al.*, 2012). While we cannot conclude for a direct or indirect role of Upa1 in Cse4-R37 methylation, our result showing ~40% reduction in Cse4-R37 methylation in *upa1Δ* strains suggests the involvement of additional methyltransferase(s) in methylation of Cse4-R37. The involvement of multiple methyltransferases in methylation of a single substrate and the ubiquity of coordinated translational methylation machinery have been reported from budding yeast and other organisms (Young *et al.*, 2012). For example, Rpl12ab in budding yeast is known to be methylated by three methyltransferases namely Rmt2, Rkms2, and Ntm1 (Chern *et al.*, 2002; Webb *et al.*, 2008; Webb *et al.*, 2010). Likewise, evolutionarily conserved eukaryotic elongation factor 1A (eEF1A) has been shown to be methylated by two different methyltransferases (Lipson *et al.*, 2010). Our studies also provide an exciting opportunity for the identification and characterization of additional methyltransferases as well as potential demethylases that differentially regulate the methylation status of Cse4 during the cell cycle.

In summary, this study is the first report describing cell cycle regulated methylation of Cse4-R37 with maximum enrichment in mitotic cells. The analysis of a mutant mimicking methylated Cse4-R37 enabled us to demonstrate that the misregulation of methylation on Cse4-R37 contributes to defects in kinetochore function and CIN. We have also defined a role for SPOUT methyltransferase Upa1 in methylation of Cse4-R37. These studies are important from an evolutionary standpoint, as consistent with our observations for cell cycle-dependent methylation of Cse4-R37 in budding yeast, methylation of CENP-A with maximum enrichment during mitosis has been reported in human cells (Sathyan *et al.*, 2017). Moreover, CENP-A methylation is catalyzed by the enzyme NRMT, and methylation of CENP-A regulates kinetochore integrity and cell survival (Sathyan *et al.*, 2017; Srivastava and Foltz, 2018; Srivastava *et al.*, 2018). Because the molecular function of Cse4/CENP-A is evolutionarily conserved, our studies from budding yeast will help us better understand the physiological significance of methylation of kinetochore proteins for high-fidelity chromosome segregation and how errors in these pathways contribute to CIN observed in many cancers.

MATERIALS AND METHODS

Yeast strains and plasmids

The yeast strains and plasmids used in this study are listed in Table 1. Strains were grown in yeast peptone dextrose (YPD; 1% yeast extract, 2% Bacto-peptone, 2% glucose) or in synthetic minimal medium with required carbon source and amino acids dropout depending on the plasmid selection.

Production of Cse4 methylarginine 37 antibodies

We generated methylarginine 37 specific Cse4 antibodies (α-^{Me}Cse4-R37) using peptides corresponding to the Cse4-R37 site with N-terminal cysteine residues (H_2N-CQQSIND(R^{Me})AL-amide). Polyclonal antibodies were raised against the conjugated methyl-peptide in rabbits by New England Peptide (Gardner, MA) and affinity purified.

Cell cycle synchronization experiments

Strains were grown in YPD or in selective media to early logarithmic phase at 25°C and were synchronized in G1 with 3-μM α-factor treatment (RP01002, GenScript), S-phase with 0.2-M hydroxyurea (HU, H8627, Sigma) or G2/M with 20-μg/mL nocodazole (NOC, M1404, Sigma) for 2 h. For G1 arrest-release experiments, strains were grown in YPD to early logarithmic phase at 25°C, synchronized in G1 with α-factor and released into pheromone-free YPD medium. α-factor was readded at 80 min after release to block cells in next G1. Samples were taken at time points after release from G1. Flow cytometry was done to verify the cell cycle synchronization using a BD FACSort flow cytometer and Cell Quest software (BD Biosciences, Boston, MA). The cell cycle stages were determined based on nuclear position and cell morphology of the cells by visual examination under the Zeiss Axioskop 2 microscope (Carl Zeiss) as described (Calvert and Lannigan, 2010).

Protein extractions, immunoprecipitation (IP), and Western blotting

Total protein extracts were made using the Trichloroacetic Acid (TCA) protein-precipitation approach (Kastenmayer *et al.*, 2005), and the levels of protein were determined using Bio-Rad DC protein quantitation assay (Bio-Rad Laboratories, Hercules, CA). IP experiments were performed to enrich Cse4 from whole-cell extracts using methodologies as described previously (Boeckmann *et al.*, 2013). Briefly, cells were dissolved in lysis buffer (0.1-M Tris pH 8.0, 6-M guanidine chloride, 0.5-N NaCl, 10-mM N-ethylmaleimide, NEM) and disrupted by glass beads in a FastPrep-5G bead beating system (SKU: 116005500, MP Biomedical). Protein extracts were clarified by centrifugation and incubated with Ni-NTA Superflow agarose (30410, Qiagen) at 4°C for 16 h. Incubated agarose samples were washed once with the lysis buffer followed by three washes with the washing buffer (25-mM Tris pH 8.0, 10-mM NEM, 0.3-M NaCl, 0.1% NP-40). Proteins bound to Ni-NTA agarose were eluted in 1 × Laemmli buffer. Protein samples were fractionated by SDS–PAGE on 4–12% Bis-TRIS SDS-polyacrylamide gels, transferred to nitrocellulose membrane, and Western blot analysis was done as described (Boeckmann *et al.*, 2013). Primary antibodies for Western blotting were α-HA (12CA5, Roche), α-^{Me}Cse4-R37 (custom made by the Basrai laboratory), α-Myc (M4439, Sigma Aldrich), α-Mif2 (a gift from Pam Meluh), α-Ctf19 (a gift from Arshad Desai) and α-Tub2 (custom made by the Basrai laboratory). Secondary antibodies were HRP-conjugated α-rabbit IgG (NA934V) and HRP-conjugated α-mouse IgG (NA931V) (Thermo Fisher Scientific).

ChIP and qPCR experiments

ChIP was done in three biological replications using the procedure as described (Mishra *et al.*, 2007; Mishra *et al.*, 2011). Strains were grown in YPD at 25°C and synchronized in G2/M with nocodazole (20-μg/mL nocodazole) for 2 h. Protein–DNA complexes were captured using α-HA agarose (A2095, Sigma Aldrich), α-Myc agarose (A7470, Sigma Aldrich), α-^{Me}Cse4-R37 (custom made by the Basrai laboratory), α-Mif2 (a gift from Pam Meluh), and α-Ctf19 (a gift from Arshad Desai) antibodies, washed and processed as previously described (Mishra *et al.*, 2007; Mishra *et al.*, 2011). ChIP-qPCR was done with Fast SYBR Green Master Mix in a 7500 Fast Real Time PCR System (Applied Biosystems, Foster City, CA) using primer sequences for *CEN1*, *CEN3*, and *ACT1* as described (Mishra *et al.*, 2021) and amplification conditions: 95°C for 20 s, followed by 40 cycles of 95°C for 3 s, 60°C for 30 s. The enrichment was calculated as percent input from three biological replicates using the $\Delta\Delta C_T$ method (Livak and Schmittgen, 2001).

SGA and tetrad analysis

Yeast strain carrying *cse4-R37F* only copy in the genome integrated at its endogenous locus and expressed from its native promoter was used to examine synthetic fitness defects with deletions of nonessential genes and essential genes. SGA screens were performed at 26°C following the procedures for generating the haploid double mutant array (Costanzo *et al.*, 2016). The data were processed and scored as described previously (Baryshnikova *et al.*, 2010; Wagih *et al.*, 2013). Tetrad dissection of genetic crosses of *cse4-R37F* with isogenic BY4741 strains carrying deletions of nonessential or mutations of essential genes were performed following the budding yeast mating and spore analysis procedures (Mortimer and Hawthorne, 1975).

Cell biology and microscopic assays

Wild-type (GFP-Cse4) and mutant strains (GFP-cse4-R37A and GFP-cse4-R37F) were grown in synthetic complete media. Cells were imaged using a Zeiss Axioimager Z2 microscope after exciting the GFP signals by the Zeiss Colibri LED illumination system (Carl Zeiss). The fluorescence intensity of Cse4-GFP and its mutants were determined by running an automatic foci quantification plugin (Fociquant) in Image J (Schneider *et al.*, 2012) and data were analyzed statistically using RStudio software (https://www.rstudio.com/). FRAP experiments were performed in metaphase cells of wild type (GFP-Cse4) and cse4-R37F (GFP-cse4-R37F) selected from logarithmically

(A) Saccharomyces cerevisiae strains:		
Strain	**Genotype**	**Reference**
YPH1015	MATa ura3-52 lys2-801 ade2-101 trp1Δ63 his3Δ200 leu2Δ1 CFIII (CEN3L.YPH278) HIS3 SUP11	Phil Hieter
YMB7287	MATa ura3Δ0 leu2Δ0 his3Δ1 met15Δ0 cse4Δ::KAN pRS416-6His-3HA-cse4-R37A	This study
YMB7289	MATa ura3Δ0 leu2Δ0 his3Δ1 met15Δ0 cse4Δ::KAN pRS416-CSE4 (pRB199)	This study
YMB8121	MATα his3Δ1 leu2Δ0 ura3Δ0 met15Δ0 lyp1Δ can1Δ::STE2pr-SpHIS5 cse4Δ::3HA-cse4R37F::mx4NAT	This study
YMB10574	MATa ura3Δ0 leu2Δ0 his3Δ1 met15Δ0 cse4Δ::6His-3HA-CSE4::mx4NAT	Basrai Lab
YMB11649	MATa ura3-52 lys2-801 ade2-101 trp1Δ63 his3Δ200 leu2Δ1 CFIII (CEN3L.YPH278) HIS3 SUP11 cse4Δ::6His-3HA-cse4R37A::mx4NAT	This study
YMB11650	MATa ura3-52 lys2-801 ade2-101 trp1Δ63 his3Δ200 leu2Δ1 CFIII (CEN3L.YPH278) HIS3 SUP11 cse4Δ::6His-3HA-cse4R37F::mx4NAT	This study
YMB11651	MATa ura3Δ0 leu2Δ0 his3Δ1 met15Δ0 cse4Δ::6His-3HA-cse4R37A::mx4NAT	This study
YMB11652	MATa ura3Δ0 leu2Δ0 his3Δ1 met15Δ0 cse4Δ::6His-3HA-cse4R37F::mx4NAT	This study
YMB11757	MATa ura3-52 lys2-801 ade2-101 trp1Δ63 his3Δ200 leu2Δ1 CFIII (CEN3L.YPH278) HIS3 SUP11 cse4Δ::6His-3HA-cse4R37K::mx4NAT	This study
YMB11828	MATa ura3Δ0 leu2Δ0 his3Δ1 met15Δ0 6His-3HA-CSE4::mx4NAT Ame1-Myc	This study
YMB11829	MATa ura3Δ0 leu2Δ0 his3Δ1 met15Δ0 6His-3HA-CSE4-R37A::mx4NAT Ame1-Myc	This study
YMB11830	MATa ura3Δ0 leu2Δ0 his3Δ1 met15Δ0 6His-3HA-CSE4-R37F::mx4NAT Ame1-Myc	This study
YMB11832	MATa his3Δ1 leu2Δ0 met15Δ0 ura3Δ0 6His-3HA-CSE4::mx4NAT upa1Δ::HIS3	This study
YMB11878	MATa his3Δ1 leu2Δ0 met15Δ0 ura3Δ0 6His-3HA-CSE4::mx4NAT pMB433 (GAL URA3 vector)	This study
YMB11879	MATa his3Δ1 leu2Δ0 met15Δ0 ura3Δ0 6His-3HA-CSE4::mx4NAT GAL1-6HIS-HA-UPA1::URA3 (mORF)	This study
YMB11880	MATa his3Δ1 leu2Δ0 met15Δ0 ura3Δ0 6His-3HA-CSE4::mx4NAT pRS425 (LEU2, 2μ vector)	This study
YMB11881	MATa his3Δ1 leu2Δ0 met15Δ0 ura3Δ0 6His-3HA-CSE4::mx4NAT upa1Δ::HIS3 pRS425 (LEU2,2μ vector)	This study
YMB11882	MATa his3Δ1 leu2Δ0 met15Δ0 ura3Δ0 6His-3HA-CSE4::mx4NAT upa1Δ::HIS3 UPA1::LEU2, 2μ	This study
YMB12214	MATa ura3-52 lys2-801 ade2-101 trp1Δ63 his3Δ200 leu2Δ1 CFIII (CEN3L.YPH278) HIS3 SUP11 pMB433 (GAL URA3 vector)	This study
YMB12215	MATa ura3-52 lys2-801 ade2-101 trp1Δ63 his3Δ200 leu2Δ1 CFIII (CEN3L.YPH278) HIS3 SUP11 GAL1-6HIS-HA-UPA1::URA3 (mORF)	This study
YMB12217	MATa ura3-52 lys2-801 ade2-101 trp1Δ63 his3Δ200 leu2Δ1 CFIII (CEN3L.YPH278) HIS3 SUP11 cse4Δ::6His-3HA-cse4R37A::mx4NAT pMB433 (GAL URA3 vector)	This study
YMB12218	MATa ura3-52 lys2-801 ade2-101 trp1Δ63 his3Δ200 leu2Δ1 CFIII (CEN3L.YPH278) HIS3 SUP11 cse4Δ::6His-3HA-cse4R37A::mx4NAT GAL1-6HIS-HA-UPA1::URA3 (mORF)	This study
BY4741	MATa ura3Δ0 leu2Δ0 his3Δ1 met15Δ0	Open Biosystems
T785	MATa leu2Δ0 his3Δ1 ura3Δ0 met15Δ0 GFP-CSE4::HISMX	This study
T786	MATa leu2Δ0 his3Δ1 ura3Δ0 met15Δ0 GFP-cse4-R37A::HISMX	This study
T796	MATa leu2Δ0 his3Δ1 ura3Δ0 met15Δ0 GFP-cse4-R37F::HISMX	This study
(B) List of plasmids:		
Plasmid	**Description**	**Reference**
pRS425	Vector::LEU2 2μ	Basrai Lab
pUPA1	UPA1::LEU2 2μ	Boone Lab
pRB199	CEN 6HIS-3HA-CSE4::URA3	R. Baker
pMB433	Vector GAL1::URA3	Basrai Lab
pGAL1 UPA1	GAL1-6HIS-3HA-UPA1::URA3	Open Biosystems

TABLE 1: List of strains and plasmids used in this investigation.

growing cultures based on the position of kinetochores (Cse4-GFP) and spindle pole bodies (Spc29-RFP) as described previously (Chen *et al.*, 2000; Maddox *et al.*, 2000). The GFP-Cse4 intensity values were statistically analyzed using a pairwise *t* test in the GraphPad Prism (Dotmatics, MA).

Chromosome segregation assays

The frequency of errors in chromosome segregation was measured by a colony color assay as described previously (Spencer *et al.*, 1990). In this assay, the loss of a reporter mini-CF led to the formation of red-sectored colonies instead of a white colony. Strains containing CF were grown to the logarithmic phase in medium selecting for the CF and plated on synthetic complete medium with limiting adenine at 25°C. The frequency of CF loss was calculated by counting the colonies that showed at least half or more than half red-sectors and were normalized to the total number of colonies. About 1000 colonies were examined for each strain from three independent transformants.

ACKNOWLEDGMENTS

We are highly thankful to Arshad Desai for Ctf19 antibodies, Pam Meluh for Mif2 antibodies, Kathy McKinnon of the National Cancer Institute Vaccine Branch FACS Core for assistance with flow cytometry, and the members of the Basrai laboratory for technical assistance and helpful discussions. P.K.M., W.C.A., P.C., L.B., Y.T., and M.A.B. were supported by the Intramural Research Program of the National Cancer Institute, National Institutes of Health; K.B. and J.S. were supported by NIH grant (R37 GM32238); N.A. and P.H.T. were supported by the Queen Mary University of London and the Biotechnology and Biological Sciences Research Council (BB/R00868X/1 and BB/T017716/1); and M.C. and C.B. were supported by the NIH grant (RO1 HG005853), and Canadian Institutes of Health Research grant (PJT-180285).

REFERENCES

Allshire RC, Karpen GH (2008). Epigenetic regulation of centromeric chromatin: old dogs, new tricks? Nat Rev Genet 9, 923–937.

Anedchenko EA, Samel-Pommerencke A, Tran Nguyen TM, Shahnejat-Bushehri S, Popsel J, Lauster D, Herrmann A, Rappsilber J, Cuomo A, Bonaldi T, Ehrenhofer-Murray AE (2019). The kinetochore module Okp1(CENP-Q)/Ame1(CENP-U) is a reader for N-terminal modifications on the centromeric histone Cse4(CENP-A). EMBO J 38, e98991.

Angrand G, Quillevere A, Loaec N, Dinh VT, Le Senechal R, Chennoufi R, Duchambon P, Keruzore M, Martins RP, Teulade-Fichou MP, *et al.* (2022). Type I arginine methyltransferases are intervention points to unveil the oncogenic Epstein-Barr virus to the immune system. Nucleic Acids Res 50, 11799–11819.

Au WC, Dawson AR, Rawson DW, Taylor SB, Baker RE, Basrai MA (2013). A novel role of the N terminus of budding yeast histone H3 variant Cse4 in ubiquitin-mediated proteolysis. Genetics 194, 513–518.

Au WC, Zhang T, Mishra PK, Eisenstatt JR, Walker RL, Ocampo J, Dawson A, Warren J, Costanzo M, Baryshnikova A, *et al.* (2020). Skp, Cullin, F-box (SCF)-Met30 and SCF-Cdc4-mediated proteolysis of CENP-A prevents mislocalization of CENP-A for chromosomal stability in budding yeast. PLoS Genet 16, e1008597.

Bakhoum SF, Swanton C (2014). Chromosomal instability, aneuploidy, and cancer. Front Oncol 4, 161.

Baryshnikova A, Costanzo M, Kim Y, Ding H, Koh J, Toufighi K, Youn JY, Ou J, San Luis BJ, Bandyopadhyay S, *et al.* (2010). Quantitative analysis of fitness and genetic interactions in yeast on a genome scale. Nat Methods 7, 1017–1024.

Bikkavilli RK, Malbon CC (2011). Arginine methylation of G3BP1 in response to Wnt3a regulates beta-catenin mRNA. J Cell Sci 124, 2310–2320.

Bloom K, Costanzo V (2017). Centromere structure and function. Prog Mol Subcell Biol 56, 515–539.

Boeckmann L, Takahashi Y, Au WC, Mishra PK, Choy JS, Dawson AR, Szeto MY, Waybright TJ, Heger C, McAndrew C, *et al.* (2013). Phosphorylation of centromeric histone H3 variant regulates chromosome segregation in Saccharomyces cerevisiae. Mol Biol Cell 24, 2034–2044.

Brown MT, Goetsch L, Hartwell LH (1993). MIF2 is required for mitotic spindle integrity during anaphase spindle elongation in Saccharomyces cerevisiae. J Cell Biol 123, 387–403.

Bui M, Walkiewicz MP, Dimitriadis EK, Dalal Y (2013). The CENP-A nucleosome: a battle between Dr Jekyll and Mr Hyde. Nucleus 4, 37–42.

Burrack LS, Berman J (2012). Flexibility of centromere and kinetochore structures. Trends Genet 28, 204–212.

Calvert ME, Lannigan J (2010). Yeast cell cycle analysis: combining DNA staining with cell and nuclear morphology. Curr Protoc Cytom Chapter 9:Unit 9:32, 31–16.

Chen Y, Baker RE, Keith KC, Harris K, Stoler S, Fitzgerald-Hayes M (2000). The N terminus of the centromere H3-like protein Cse4p performs an essential function distinct from that of the histone fold domain. Mol Cell Biol 20, 7037–7048.

Chern MK, Chang KN, Liu LF, Tam TC, Liu YC, Liang YL, Tam MF (2002). Yeast ribosomal protein L12 is a substrate of protein-arginine methyltransferase 2. J Biol Chem 277, 15345–15353.

Clarke L, Carbon J (1980). Isolation of a yeast centromere and construction of functional small circular chromosomes. Nature 287, 504–509.

Clarke PR (2021). Keep it focused: PRMT6 drives the localization of RCC1 to chromosomes to facilitate mitosis, cell proliferation, and tumorigenesis. Mol Cell 81, 1128–1129.

Cohen RL, Espelin CW, De Wulf P, Sorger PK, Harrison SC, Simons KT (2008). Structural and functional dissection of Mif2p, a conserved DNA-binding kinetochore protein. Mol Biol Cell 19, 4480–4491.

Costanzo M, Baryshnikova A, Bellay J, Kim Y, Spear ED, Sevier CS, Ding H, Koh JL, Toufighi K, Mostafavi S, *et al.* (2010). The genetic landscape of a cell. Science 327, 425–431.

Costanzo M, VanderSluis B, Koch EN, Baryshnikova A, Pons C, Tan G, Wang W, Usaj M, Hanchard J, Lee SD, *et al.* (2016). A global genetic interaction network maps a wiring diagram of cellular function. Science 353, aaf1420.

Dillon MB, Rust HL, Thompson PR, Mowen KA (2013). Automethylation of protein arginine methyltransferase 8 (PRMT8) regulates activity by impeding S-adenosylmethionine sensitivity. J Biol Chem 288, 27872–27880.

Fang L, Zhang L, Wei W, Jin X, Wang P, Tong Y, Li J, Du JX, Wong J (2014). A methylation-phosphorylation switch determines Sox2 stability and function in ESC maintenance or differentiation. Mol Cell 55, 537–551.

Fischbock-Halwachs J, Singh S, Potocnjak M, Hagemann G, Solis-Mezarino V, Woike S, Ghodgaonkar-Steger M, Weissmann F, Gallego LD, Rojas J, *et al.* (2019). The COMA complex interacts with Cse4 and positions Sli15/Ipl1 at the budding yeast inner kinetochore. eLife 8, e42879.

Haase J, Mishra PK, Stephens A, Haggerty R, Quammen C, Taylor RM 2nd, Yeh E, Basrai MA, Bloom K (2013). A 3D map of the yeast kinetochore reveals the presence of core and accessory centromere-specific histone. Curr Biol 23, 1939–1944.

Hara M, Fukagawa T (2020). Dynamics of kinetochore structure and its regulations during mitotic progression. Cell Mol Life Sci 77, 2981–2995.

He W, Ma X, Yang X, Zhao Y, Qiu J, Hang H (2011). A role for the arginine methylation of Rad9 in checkpoint control and cellular sensitivity to DNA damage. Nucleic Acids Res 39, 4719–4727.

Henikoff S, Ahmad K, Platero JS, van Steensel B (2000). Heterochromatic deposition of centromeric histone H3-like proteins. Proc Natl Acad Sci USA 97, 716–721.

Henikoff S, Furuyama T (2010). Epigenetic inheritance of centromeres. Cold Spring Harb Symp Quant Biol 75, 51–60.

Henikoff S, Furuyama T (2012). The unconventional structure of centromeric nucleosomes. Chromosoma 121, 341–352.

Hewawasam G, Shivaraju M, Mattingly M, Venkatesh S, Martin-Brown S, Florens L, Workman JL, Gerton JL (2010). Psh1 is an E3 ubiquitin ligase that targets the centromeric histone variant Cse4. Mol Cell 40, 444–454.

Ho KH, Tsuchiya D, Oliger AC, Lacefield S (2014). Localization and function of budding yeast CENP-A depends upon kinetochore protein interactions and is independent of canonical centromere sequence. Cell Rep 9, 2027–2033.

Hoffmann G, Samel-Pommerencke A, Weber J, Cuomo A, Bonaldi T, Ehrenhofer-Murray AE (2018). A role for CENP-A/Cse4 phosphorylation on serine 33 in deposition at the centromere. FEMS Yeast Res 18.

Horlbeck MA, Xu A, Wang M, Bennett NK, Park CY, Bogdanoff D, Adamson B, Chow ED, Kampmann M, Peterson TR, *et al.* (2018). Mapping the genetic landscape of human cells. Cell 174, 953–967.e922.

Hornung P, Troc P, Malvezzi F, Maier M, Demianova Z, Zimniak T, Litos G, Lampert F, Schleiffer A, Brunner M, *et al*. (2014). A cooperative mechanism drives budding yeast kinetochore assembly downstream of CENP-A. J Cell Biol 206, 509–524.

Huang CC, Chang KM, Cui H, Jayaram M (2011). Histone H3-variant Cse4-induced positive DNA supercoiling in the yeast plasmid has implications for a plasmid origin of a chromosome centromere. Proc Natl Acad Sci USA 108, 13671–13676.

Huang T, Yang Y, Song X, Wan X, Wu B, Sastry N, Horbinski CM, Zeng C, Tiek D, Goenka A, *et al*. (2021). PRMT6 methylation of RCC1 regulates mitosis, tumorigenicity, and radiation response of glioblastoma stem cells. Mol Cell 81, 1276–1291.e9.

Ismail S, Flemming D, Thoms M, Gomes-Filho JV, Randau L, Beckmann R, Hurt E (2022). Emergence of the primordial pre-60S from the 90S pre-ribosome. Cell Rep 39, 110640.

Jiang W, Middleton K, Yoon HJ, Fouquet C, Carbon J (1993). An essential yeast protein, CBF5p, binds in vitro to centromeres and microtubules. Mol Cell Biol 13, 4884–4893.

Kastenmayer JP, Lee MS, Hong AL, Spencer FA, Basrai MA (2005). The C-terminal half of Saccharomyces cerevisiae Mad1p mediates spindle checkpoint function, chromosome transmission fidelity and CEN association. Genetics 170, 509–517.

Keith KC, Baker RE, Chen Y, Harris K, Stoler S, Fitzgerald-Hayes M (1999). Analysis of primary structural determinants that distinguish the centromere-specific function of histone variant Cse4p from histone H3. Mol Cell Biol 19, 6130–6139.

Krishnamohan A, Jackman JE (2019). A family divided: distinct structural and mechanistic features of the SpoU-TrmD (SPOUT) methyltransferase superfamily. Biochemistry 58, 336–345.

Krogan NJ, Peng WT, Cagney G, Robinson MD, Haw R, Zhong G, Guo X, Zhang X, Canadien V, Richards DP, *et al*. (2004). High-definition macromolecular composition of yeast RNA-processing complexes. Mol Cell 13, 225–239.

Lawrimore J, Bloom K (2019). The regulation of chromosome segregation via centromere loops. Crit Rev Biochem Mol Biol 54, 352–370.

Lawrimore J, Doshi A, Friedman B, Yeh E, Bloom K (2018). Geometric partitioning of cohesin and condensin is a consequence of chromatin loops. Mol Biol Cell 29, 2737–2750.

Lipson RS, Webb KJ, Clarke SG (2010). Two novel methyltransferases acting upon eukaryotic elongation factor 1A in Saccharomyces cerevisiae. Arch Biochem Biophys 500, 137–143.

Liu N, Yang R, Shi Y, Chen L, Liu Y, Wang Z, Liu S, Ouyang L, Wang H, Lai W, *et al*. (2020). The cross-talk between methylation and phosphorylation in lymphoid-specific helicase drives cancer stem-like properties. Signal Transduct Target Ther 5, 197.

Livak KJ, Schmittgen TD (2001). Analysis of relative gene expression data using real-time quantitative PCR and the 2(-Delta Delta C(T)) Method. Methods 25, 402–408.

Ma L, Ho K, Piggott N, Luo Z, Measday V (2012). Interactions between the kinetochore complex and the protein kinase A pathway in Saccharomyces cerevisiae. G3 (Bethesda) 2, 831–841.

Maddox PS, Bloom KS, Salmon ED (2000). The polarity and dynamics of microtubule assembly in the budding yeast Saccharomyces cerevisiae. Nat Cell Biol 2, 36–41.

Maeda M, Hasegawa H, Sugiyama M, Hyodo T, Ito S, Chen D, Asano E, Masuda A, Hasegawa Y, Hamaguchi M, Senga T (2016). Arginine methylation of ubiquitin-associated protein 2-like is required for the accurate distribution of chromosomes. FASEB J 30, 312–323.

Meluh PB, Koshland D (1995). Evidence that the MIF2 gene of Saccharomyces cerevisiae encodes a centromere protein with homology to the mammalian centromere protein CENP-C. Mol Biol Cell 6, 793–807.

Meluh PB, Yang P, Glowczewski L, Koshland D, Smith MM (1998). Cse4p is a component of the core centromere of Saccharomyces cerevisiae. Cell 94, 607–613.

Mishra PK, Au WC, Choy JS, Kuich PH, Baker RE, Foltz DR, Basrai MA (2011). Misregulation of Scm3p/HJURP causes chromosome instability in Saccharomyces cerevisiae and human cells. PLoS Genet 7, e1002303.

Mishra PK, Basrai MA (2019). Protein kinases in mitotic phosphorylation of budding yeast CENP-A. Curr Genet 65, 1325–1332.

Mishra PK, Baum M, Carbon J (2007). Centromere size and position in Candida albicans are evolutionarily conserved independent of DNA sequence heterogeneity. Mol Genet Genomics 278, 455–465.

Mishra PK, Guo J, Dittman LE, Haase J, Yeh E, Bloom K, Basrai MA (2015). Pat1 protects centromere-specific histone H3 variant Cse4 from Psh1-mediated ubiquitination. Mol Biol Cell 26, 2067–2079.

Mishra PK, Olafsson G, Boeckmann L, Westlake TJ, Jowhar ZM, Dittman LE, Baker RE, D'Amours D, Thorpe PH, Basrai MA (2019). Cell cycle-dependent association of polo kinase Cdc5 with CENP-A contributes to faithful chromosome segregation in budding yeast. Mol Biol Cell 30, 1020–1036.

Mishra PK, Ottmann AR, Basrai MA (2013). Structural integrity of centromeric chromatin and faithful chromosome segregation requires Pat1. Genetics 195, 369–379.

Mishra PK, Wood H, Stanton J, Au WC, Eisenstatt JR, Boeckmann L, Sclafani RA, Weinreich M, Bloom KS, Thorpe PH, Basrai MA (2021). Cdc7-mediated phosphorylation of Cse4 regulates high-fidelity chromosome segregation in budding yeast. Mol Biol Cell 32, ar15.

Mortimer RK, Hawthorne DC (1975). Genetic mapping in yeast. Methods Cell Biol 11, 221–233.

Mostaqul Huq MD, Gupta P, Tsai NP, White R, Parker MG, Wei LN (2006). Suppression of receptor interacting protein 140 repressive activity by protein arginine methylation. EMBO J 25, 5094–5104.

Musacchio A, Desai A (2017). A molecular view of kinetochore assembly and function. Biology (Basel) 6, 5.

Nguyen TMT, Munhoven A, Samel-Pommerencke A, Kshirsagar R, Cuomo A, Bonaldi T, Ehrenhofer-Murray AE (2023). Methylation of CENP-A/Cse4 on arginine 143 and lysine 131 regulates kinetochore stability in yeast. Genetics 223, iyad028.

Ohkuni K, Takahashi Y, Fulp A, Lawrimore J, Au WC, Pasupala N, Levy-Myers R, Warren J, Strunnikov A, Baker RE, *et al*. (2016). SUMO-Targeted Ubiquitin Ligase (STUbL) Slx5 regulates proteolysis of centromeric histone H3 variant Cse4 and prevents its mislocalization to euchromatin. Mol Biol Cell 27, 1500–1510.

Ohta S, Wood L, Toramoto I, Yagyu K, Fukagawa T, Earnshaw WC (2015). CENP-32 is required to maintain centrosomal dominance in bipolar spindle assembly. Mol Biol Cell 26, 1225–1237.

Paik WK, Paik DC, Kim S (2007). Historical review: the field of protein methylation. Trends Biochem Sci 32, 146–152.

Pearson CG, Yeh E, Gardner M, Odde D, Salmon ED, Bloom K (2004). Stable kinetochore-microtubule attachment constrains centromere positioning in metaphase. Curr Biol 14, 1962–1967.

Ranjitkar P, Press MO, Yi X, Baker R, MacCoss MJ, Biggins S (2010). An E3 ubiquitin ligase prevents ectopic localization of the centromeric histone H3 variant via the centromere targeting domain. Mol Cell 40, 455–464.

Samel A, Cuomo A, Bonaldi T, Ehrenhofer-Murray AE (2012). Methylation of CenH3 arginine 37 regulates kinetochore integrity and chromosome segregation. Proc Natl Acad Sci USA 109, 9029–9034.

Santaguida S, Amon A (2015). Short- and long-term effects of chromosome mis-segregation and aneuploidy. Nat Rev Mol Cell Biol 16, 473–485.

Sathyan KM, Fachinetti D, Foltz DR (2017). alpha-amino trimethylation of CENP-A by NRMT is required for full recruitment of the centromere. Nat Commun 8, 14678.

Schneider CA, Rasband WS, Eliceiri KW (2012). NIH Image to ImageJ: 25 years of image analysis. Nat Methods 9, 671–675.

Schwer B, Erdjument-Bromage H, Shuman S (2011). Composition of yeast snRNPs and snoRNPs in the absence of trimethylguanosine caps reveals nuclear cap binding protein as a gained U1 component implicated in the cold-sensitivity of tgs1Δ cells. Nucleic Acids Res 39, 6715–6728.

Smith DL, Erce MA, Lai YW, Tomasetig F, Hart-Smith G, Hamey JJ, Wilkins MR (2020). Crosstalk of phosphorylation and arginine methylation in disordered SRGG repeats of Saccharomycescerevisiae fibrillarin and its association with nucleolar localization. J Mol Biol 432, 448–466.

Snider CE, Stephens AD, Kirkland JG, Hamdani O, Kamakaka RT, Bloom K (2014). Dyskerin, tRNA genes, and condensin tether pericentric chromatin to the spindle axis in mitosis. J Cell Biol 207, 189–199.

Spencer F, Gerring SL, Connelly C, Hieter P (1990). Mitotic chromosome transmission fidelity mutants in Saccharomyces cerevisiae. Genetics 124, 237–249.

Sprague BL, Pearson CG, Maddox PS, Bloom KS, Salmon ED, Odde DJ (2003). Mechanisms of microtubule-based kinetochore positioning in the yeast metaphase spindle. Biophys J 84, 3529–3546.

Srivastava S, Foltz DR (2018). Posttranslational modifications of CENP-A: marks of distinction. Chromosoma 127, 279–290.

Srivastava S, Zasadzinska E, Foltz DR (2018). Posttranslational mechanisms controlling centromere function and assembly. Curr Opin Cell Biol 52, 126–135.

Stoler S, Keith KC, Curnick KE, Fitzgerald-Hayes M (1995). A mutation in CSE4, an essential gene encoding a novel chromatin-associated protein in yeast, causes chromosome nondisjunction and cell cycle arrest at mitosis. Genes Dev 9, 573–586.

Sullivan KF, Hechenberger M, Masri K (1994). Human CENP-A contains a histone H3 related histone fold domain that is required for targeting to the centromere. J Cell Biol 127, 581–592.
Takahashi K, Chen ES, Yanagida M (2000). Requirement of Mis6 centromere connector for localizing a CENP-A-like protein in fission yeast. Science 288, 2215–2219.
Verdaasdonk JS, Bloom K (2011). Centromeres: unique chromatin structures that drive chromosome segregation. Nat Rev Mol Cell Biol 12, 320–332.
Vlijm R, Kim SH, De Zwart PL, Dalal Y, Dekker C (2017). The supercoiling state of DNA determines the handedness of both H3 and CENP-A nucleosomes. Nanoscale 9, 1862–1870.
Wagih O, Usaj M, Baryshnikova A, VanderSluis B, Kuzmin E, Costanzo M, Myers CL, Andrews BJ, Boone CM, Parts L (2013). SGAtools: one-stop analysis and visualization of array-based genetic interaction screens. Nucleic Acids Res 41, W591–596.
Wang YC, Huang SH, Chang CP, Li C (2023). Identification and characterization of glycine- and arginine-rich motifs in proteins by a novel GAR motif finder program. Genes (Basel) 14, 330.
Watanabe Y (2012). Geometry and force behind kinetochore orientation: lessons from meiosis. Nat Rev Mol Cell Biol 13, 370–382.
Webb KJ, Laganowsky A, Whitelegge JP, Clarke SG (2008). Identification of two SET domain proteins required for methylation of lysine residues in yeast ribosomal protein Rpl42ab. J Biol Chem 283, 35561–35568.
Webb KJ, Lipson RS, Al-Hadid Q, Whitelegge JP, Clarke SG (2010). Identification of protein N-terminal methyltransferases in yeast and humans. Biochemistry 49, 5225–5235.
Wisniewski J, Hajj B, Chen J, Mizuguchi G, Xiao H, Wei D, Dahan M, Wu C (2014). Imaging the fate of histone Cse4 reveals de novo replacement in S phase and subsequent stable residence at centromeres. eLife 3, e02203.
Wlodarski T, Kutner J, Towpik J, Knizewski L, Rychlewski L, Kudlicki A, Rowicka M, Dziembowski A, Ginalski K (2011). Comprehensive structural and substrate specificity classification of the Saccharomyces cerevisiae methyltransferome. PLoS One 6, e23168.
Yan WW, Liang YL, Zhang QX, Wang D, Lei MZ, Qu J, He XH, Lei QY, Wang YP (2018). Arginine methylation of SIRT7 couples glucose sensing with mitochondria biogenesis. EMBO Rep 19, e46377.
Yeh E, Haase J, Paliulis LV, Joglekar A, Bond L, Bouck D, Salmon ED, Bloom KS (2008). Pericentric chromatin is organized into an intramolecular loop in mitosis. Curr Biol 18, 81–90.
Yeh E, Yang C, Chin E, Maddox P, Salmon ED, Lew DJ, Bloom K (2000). Dynamic positioning of mitotic spindles in yeast: role of microtubule motors and cortical determinants. Mol Biol Cell 11, 3949–3961.
Young BD, Weiss DI, Zurita-Lopez CI, Webb KJ, Clarke SG, McBride AE (2012). Identification of methylated proteins in the yeast small ribosomal subunit: a role for SPOUT methyltransferases in protein arginine methylation. Biochemistry 51, 5091–5104.
Zhang K, Lin W, Latham JA, Riefler GM, Schumacher JM, Chan C, Tatchell K, Hawke DH, Kobayashi R, Dent SY (2005). The Set1 methyltransferase opposes Ipl1 aurora kinase functions in chromosome segregation. Cell 122, 723–734.
Zhong XY, Yuan XM, Xu YY, Yin M, Yan WW, Zou SW, Wei LM, Lu HJ, Wang YP, Lei QY (2018). CARM1 methylates GAPDH to regulate glucose metabolism and is suppressed in liver cancer. Cell Rep 24, 3207–3223.